

A petrogenetic model of basalts from the Northern Central Indian Ridge: 3-11°S

Dwijesh Ray^{a*}, Sridhar D. Iyer^a, Ranadip Banerjee^a, Saumitra Misra^b and Mike Widdowson^c

^aNational Institute of Oceanography, Goa-403 004, INDIA

^bDepartment of Geology and Geophysics, Indian Institute of Technology, Kharagpur-721
302, INDIA

^cDepartment of Earth Sciences, Open University, Milton Keynes, MK7 6AA, U. K.

Abstract

Mid-Ocean Ridge Basalts (MORB) from Northern Central Indian Ridge (NCIR) were recovered between latitudes 3° and 11°S and are olivine tholeiite with higher abundances of K and Rb. They are of typical transitional MORB (T-MORB) variety and appear to have been generated from an enriched mantle peridotite source. The primitive NCIR MORBs having #Mg > 0.68, are the product of partial melting at an estimated pressure of ~10 kbar. It is inferred that the magma was subsequently modified at a pressure >10 kbar by crystal fractionation and spinel was the first mineral to crystallise followed by separation of relatively Fe-rich olivine with subsequent decrease in pressure. During progressive fractionation at lower pressure (between 10-5 kbar), the bulk composition of the magma became systematically depleted in MgO, and enriched in FeO_t, TiO₂, P₂O₅ and Na₂O. There was, however, limited gradual depletion in Al₂O₃ and CaO, and concomitant enrichment in K₂O. With the progressive fractionation, these basalts became gradually enriched in V, Co, Y, Zr and to some extent in Sr, and depleted in Ni and Cr. In addition, the ΣREE of magma also increased with fractionation, without any change in (La/Yb)_N value.

Keywords: MORB, NCIR, geochemistry, petrogenesis

*Corresponding author: Dwijesh Ray. Present address: Geological Oceanography Division, National Institute of Oceanography, Goa-403 004, India. Tel: +91(0) 832-2450495, Fax: +91(0) 832-2450609

E-mail address: dwijesh@rediffmail.com (Dwijesh Ray)

1. Introduction

The Northern Central Indian Ridge (NCIR) between 3° and 11°S latitudes is joined to the north with the slow spreading Carlsberg Ridge (CR; ~24-26 mm/yr, full spreading rate) and to the south with the intermediate spreading Southern Central Indian Ridge (SCIR; ~50 mm/yr) (Fig. 1). The earlier petrological investigations of the Central Indian Ridge were concentrated either on and along the CR to the north and at the southern end of the CIR up to the Rodriguez Triple Junction (RTJ, 25°30'S/ 70°00'E) (Hekinian, 1968; Price et al., 1986; Herzig and Plüger, 1988; Humler and Whitechurch, 1988; Banerjee and Iyer, 1991, 2003; Iyer and Banerjee, 1993; Rehkamper and Hofmann, 1997, Mudholkar, 2001, Murton et al., 2005, Nauret et al., 2006). By contrast, the NCIR has been left relatively uninvestigated. During the American expeditions (*MONSOON*, 1960; *LUSIAD*, 1962-63; *DODO*, 1964; *CIRCE*, 1968 and *ANTIPODE*, 1970-71), Russian expeditions (*VITIAZ* and *AKADEMIC-KURCHATOV* cruises during 1964/65) and German expedition (by *SO-28*, 1987) ship-board researchers did some sporadic sampling along the NCIR, but this proved insufficient to characterise in detail the NCIR petrology and geochemistry. Noteworthy works on NCIR petrochemistry include the work of Engel and Fisher (1975) on various rock-types (granitic to ultramafic), whilst in more recent times Rehkamper and Hofmann (1997) published high quality trace and isotopic glass data (samples collected during *SO 28*). Most recently, Hellebrand et al. (2002) documented partial melting in NCIR peridotites as a method of determining geodynamic variables such as spreading rate and mantle temperature.

In this context, the present work attempts to reduce the long-standing gap in the existing knowledge of NCIR MORBs and provides a set of new high quality analyses for the Indian Ocean petrological database. Recent expeditions to the Indian Ocean under the InRidge Programme (Cruise R/V Sagar Kanya #125 and #165 in the year of 1997 and 2001 respectively) permitted the sampling of basalts, using chainbag dredge, from three different geographic as well as tectonic locations (Table 1, Fig.1). Here, we detail the bulk geochemistry (major, trace and REE) of the NCIR MORBs with the objective to develop a primary petrogenetic model explaining their formation history. In order to achieve this, in addition to the present geochemical dataset, previously published datasets (e.g. data collected from Petrological Database of Lamont-Doherty Geological Observatory of Columbia University or PETDB MORB database at <http://www.lamont.columbia.edu> and *SO 28* cruise report) are also integrated to draw a meaningful conclusion.

2. Sample Description and Petrography

Rocks from the location VT 4 and VT 5 (Fig. 1, inset) are homogeneous basalts, comprising fresh to moderately altered vesicular pillow lavas weighing ~64 kg, sometimes displaying a glassy crust (~5-25 mm, Mukhopadhyay et al., 1998). Rocks from the near-ridge seamount in VM area at location 9DG (Fig. 1, inset) consist of a uniform column-like basalt blocks, though in a few instances pillows were also recovered. The columns are either cylindrical or conical in shape and often have a thin veneer of glass (thickness ~3-4 mm; Droliia et al., 2003).

Petrographically the NCIR basalts are usually moderately phyrlic plagioclase-rich tholeiite (MPPB; Bougalt and Hekinian, 1974), plagioclase occurs as the dominant mineral in variable morphotypes such as phenocryst, microphenocryst, and even megacryst; and followed in abundance by olivine and pyroxene with varying proportions of groundmass materials (Pluger et al., 1988). The modal proportion of plagioclases vary a considerable range (up to 19 vol%). The modal variation for olivine is noted comparatively less (0.04-1.69%) while diopside varies the least (up to 0.05 vol%) among these three. Microscope study reveals that the newly collected basalts of the NCIR are porphyritic with a few large phenocrysts of mainly prismatic plagioclases (An_{62-90} , microprobe data, unpublished) embedded within a fine-grained groundmass of plagioclase laths (An_{35-79}), and clinopyroxene (diopside, $Wo_{45-51}En_{25-37}Fs_{14-24}$) with some interstitial glass. After plagioclase, the other major phenocryst populations include olivine (Fo_{81-88}) and, in rare instances, clinopyroxene (mainly diopside $\sim Wo_{49-51}En_{31-35}Fs_{16-18}$). The average mineral compositions of NCIR basalts are given in Table 2. Plagioclase from VM basalts display the maximum variation in aorthite content (An_{52-85}) compared to VT plagioclases (An_{64-83}). Olivine forsterite from both the areas vary from Fo_{80} to Fo_{88} . The plagioclase phenocrysts display compositional zoning (Fig. 2a), which is generally absent in groundmass plagioclase. Some tiny spherical materials, perhaps fluid/ melt inclusions, are also present within the plagioclase phenocrysts (Fig. 2b). The other common occurrence of plagioclase is as thin-slender shaped crystals, which due to their extreme development show acicular form which radiate from a common centre giving rise to spherulitic structure. The olivine phenocrysts occur as euhedral (most common) to subhedral (rare) equant grains, which are almost colourless and rarely show zoning. In a few cases, olivine shows alteration along the inherent fracture to reddish-brown iddingsite. Amphiboles occur in the VT as well as in VM basalts but only as poorly pleochroic subhedral grains closely associated with clinopyroxene.

The interstitial glasses in the groundmass have locally altered to brown colour chlorophite and also show devitrification. Opaques of variable shape present in the groundmass are mainly titanomagnetite (FeO_t ~46-71 wt% and TiO_2 ~13-23 wt%, Table 2). These also occur as inclusions within plagioclase phenocrysts and the glassy groundmass. Semicircular or irregular-shaped vesicles are present in the groundmass, but are generally unfilled with the exception of marginal rim-like infillings in a few samples.

3. Geochemistry

3.1. Analytical techniques

Around 50-70 gm of fresh, cleanly washed, dry chips of each basalt sample (~17 nos) of NCIR were pulverised to fine rock powder by a tungsten-carbide ring mill installed on board Sagar Kanya and at the Presidency College, Kolkata, India. The glass samples (4 nos), chipped from the surface of the VT pillow basalts were also powdered and ~10-15 gm obtained. The major element analyses of the NCIR samples including basalt (7 nos) and glassy basalts (4 nos) were carried out by XRF at the Open University, United Kingdom (ARL 8420+) and IIT, Kharagpur, India (Philips PW 2404), on fused and pressed pellets.

All the trace elements including REE (Sc, V, Cr, Co, Ni, Cu, Zn, Ga, Rb, Sr, Y, Zr, Nb, Cs, Ba, La, Ce, Pr, Nd, Sm, Eu, Gd, Tb, Dy, Ho, Er, Tm, Yb, Lu, Hf, Pb, Th and U) were determined on the same sample powders by inductively coupled plasma-mass spectrometry (ICP-MS, model ELAN DRC II, Perkin Elmer Sciex Instruments, USA) at the National Geophysical Research Institute, Hyderabad, India, following the procedure after Balaram et al. (1999). Two runs were carried out on JB-2 standard at the initial and final stages of the analyses of 21 unknown basalts of the NCIR. All the elements with atomic number between Sc and Ba show a precision better than 4.5 % and those between La and U are have a precision better than 7.5%.

3.2. Major and Trace element geochemistry

The representative whole rock chemical analyses (major, trace and REE) of the NCIR basalts from VT and VM area are presented in Table 3. Samples from the VT 4 and VT 5 areas show low LOI (loss on ignition) between ~0.12 and 0.5 wt%, while the seamount basalts (VM 9DG) have relatively higher LOI values between ~0.63 and 1.27 wt%. The average major oxide compositions of the VT basalts and glasses as well as VM basalts are compared with those of the NCIR basalts, adjacent CR and SCIR basalts (data collected from literature) and primitive MORB compositions (after Presnall and Hoover, 1987) in Table 4.

In the major oxide spiderdiagram normalised against primitive MORB (average composition after Presnall and Hoover, 1987), the NCIR basalts from literature show maximum variations of K_2O and K_2O/Na_2O ratios both in positive and negative senses (Fig. 3a). This is followed by a positive variation of TiO_2 and Na_2O and negative variation of Al_2O_3/TiO_2 . Subordinate positive variations of FeO_t and CaO/Al_2O_3 , and positive as well as negative variations of MgO are also noted, though the negative variation for MgO is more pronounced. Minor variations are also observed for Al_2O_3 and CaO .

The basalt samples from the VT and VM areas show similar type of major oxide spiderdiagrams but with some exceptions (Fig. 3b). Most of the samples show positive anomalies for K_2O and K_2O/Na_2O , which are ~ 10 and ~ 6 times higher respectively than those in the primitive MORB. Negative variation is observed only for MgO . Major element composition of glassy basalts are similar with the holocrystalline basalts, except the glassy basalts have relatively low K_2O value (0.03-0.05, Table 3).

The average NCIR, SCIR and CR basalts can efficiently be discriminated by their K_2O and K_2O/Na_2O ratios in the major oxide spiderdiagram (Fig. 3c), as these values progressively increase from NCIR (0.11, 0.04), through SCIR (0.14, 0.05) to CR basalts (0.47, 0.13). The VT and VM basalts are relatively enriched in these values compared to published NCIR data and are either intermediate between SCIR and CR basalts or similar to CR basalt in major element composition. The average NCIR, SCIR and CR basalts are very similar in SiO_2 , Al_2O_3 , FeO_t , MgO , CaO , $\#Mg$, CaO/Al_2O_3 and Al_2O_3/TiO_2 . Though some variations are noticed for TiO_2 and MnO , but these are not very systematic. The average NCIR basalt, in general, has higher Na_2O and Na_2O+K_2O compared to those in the SCIR basalt, the VM basalt particularly shows similar values to those of the CR basalt.

If $\#Mg$ is taken as a parameter to measure the evolution of the basaltic magmas, sample 33 DR 01/2 (SO 28 cruise report) can be considered as the least evolved members of the NCIR basalts (Table 4). In the major oxide spiderdiagram normalised vis-s-vis the most primitive NCIR sample (33 DR 01/2), the average NCIR, VT and VM basalts all represent evolved basaltic rock members (Fig. 3d).

The range in trace element enrichment in these samples is well illustrated in Fig. 4, where primitive mantle normalised (primitive mantle normalized data from Sun and McDonough, 1989) patterns for selected samples are shown. The basalt samples collected from VT 4, VT 5 and VM 9DG locations characteristically exhibit differential variation in their trace element concentration, while variation for Rb is recorded the maximum. The

variations for Rb are minimum in VT 5 basalts compared to adjacent VT 4 samples. Degree of large ion lithophile elemental (LIL) enrichment is the highest in VM 9DG, followed by VT 5 and VT 4 samples. For the elements between Sr and Yb, the basalts from all the three locations do not exhibit much variation. The most notable feature observed in primitive normalized multielement variation diagram is that many samples show a very obvious negative Nb-anomaly (i.e. when normalized to primitive mantle values Nb appears to be more depleted compared to its adjacent elements on either side).

3.3. Major and trace element variation

The NCIR basalts as a whole are compared to the type-I, II and III Indian Ocean Ridge Basalts (IORB) as described by Natland (1991) in TiO_2 versus Na_2O plot (Fig. 5a). In general, these basalts are compositionally similar to the type-II IORB, with a gradation towards type-III. The bulk compositional variations of the VT and VM basalts along with other NCIR basalts from literature are examined against #Mg in Figs. 5 (b-f). The #Mg is chosen as a reference parameter as it shows a wide variation in range from 0.73 to 0.49 and is widely used to examine bulk compositional variation of basaltic rocks. In the major oxide binary diagram, SiO_2 practically shows no variation with decreasing #Mg. Near horizontal or slightly increased trend is also observed for MnO while Al_2O_3 and CaO contents show a narrow but systematic decrease (within ~2-3 wt%) for all the samples with decreasing #Mg (Figs. 5c and e). The TiO_2 , Na_2O and P_2O_5 , on the other hand, show gently increasing trends with decreasing #Mg (Figs. 5 b, f, g). These oxides have increased by ~1, 1.5 and 0.20 wt% respectively, with decrease in #Mg from ~0.73 to 0.49. In contrast, K_2O shows poorly increasing trend with decreasing #Mg (Fig. h). The VT and VM basalts roughly follow the same, though they have much higher values of K_2O up to 0.8 wt% at lower #Mg between ~0.55 and 0.50 (Fig. h).

An examination of major oxide variation diagrams shows that three geochemical parameters e.g. #Mg, TiO_2 and P_2O_5 , vary systematically in the NCIR basalts and they can be used as references to examine the variations of trace element compositions of these rocks in bivariate plots. Among the transitional group of elements, Cr and Ni decrease with decreasing #Mg (Figs. 6 a, b). In the #Mg versus Cr plot, the NCIR basalts, however, only show two distinct sub-parallel trends for VM and VT samples. The VM basalts show much gentler decreasing trend for Cr than that of the VT basalt with decreasing #Mg. In the #Mg versus Ni plot the variation of Ni is same both at higher and at lower #Mg (Fig. 6a). The HFS

elements Y and Zr show similar increasing trends with decreasing #Mg, though absolute contents of these elements in the NCIR basalts are different (Figs. 6e, f).

The CI Carbonaceous chondrite normalised (after McDonough and Sun, 1995) REE spiderdiagrams of NCIR basalts are plotted in Fig. 7. The spiderdiagrams for the VT 4, VT 5 and VM 9DG basalts show flat REE patterns except for the VT 4 samples, which show a minor depletion in LREE (La, Ce, Pr) (Fig. 7a). The REE abundances in these basalts are in general ~20 to 30 times higher than the average carbonaceous chondrites (McDonough and Sun, 1995). The $(Ce/Yb)_N$ values for the VT 4 samples vary between 0.67 and 1.06, those for VT 5 samples between 1.0 and 1.08, and for the VM 9DG samples mostly between 1.02 and 1.10. The $(La/Sm)_N$ and $(Gd/Yb)_N$ values for the VT 4, VT 5 and VM 9DG samples vary between 0.46 – 0.77 and 1.15 - 1.27, 0.73 – 0.82 and 1.26 - 1.28, 0.78 - 1.9 and 1.24 - 1.44, respectively. Sample 6A of VM 9DG shows highest values for $(Ce/Yb)_N$ (2.44) and $(La/Sm)_N$ (1.9).

The NCIR basalts can further be grouped into three distinct types depending on their REE abundances - (a) basalts having highest REE (~66-72 ppm) (Group-I) and (b) basalts having lowest REE abundances (~36-42 ppm) (Group-III). There is, however, an intermediate basalt type having REE between ~45-60 ppm (Group-II). Amongst these, the Group-I basalt is most dominant (7) samples followed by Group-III (5) and Group-II (3) basalts respectively. The VT 4 basalts contain Group I and Group III combination, whereas VT 5 samples represent Group I and Group II REE only (Figs. 7a, b). All the spectrum including the three REE groups of basalts are present in near ridge seamount VM 9DG samples (Fig. 7c). One of the VM samples (# 6A), however, contains very high La and Ce, otherwise it belongs to Group II REE basalt.

The inter-relationship of these three REE groups of basalt is examined in #Mg, TiO_2 and P_2O_5 versus total REE (ΣREE) plots (Figs. 7d-f). In all of these plots the ΣREE shows linear increase either with decreasing #Mg or increasing TiO_2 and P_2O_5 . In REE character, the NCIR basalts also show gradational nature between type-II and type-III IORB of Natland (1991) (Fig. 7e).

3.4. Identification of igneous process(es)

Whether the NCIR magma has undergone significant fractional crystallization after its generation from the mantle source by partial melting is an important aspect of its petrogenesis. In major oxide variation diagrams (Fig. 5), Mg/Fe ratios of the NCIR basalts show a large variation (#Mg~0.73 to 0.49) among its bulk constituents due to crystal

fractionation. The variations of other major oxides, e.g. SiO₂ (~ 6 wt%), Al₂O₃ (~4 wt%), CaO (~2 wt%) and Na₂O (~2 wt%) are very limited in extent (Fig. 3a). Fractionation causes the maximum variation of minor oxides in TiO₂ (~1 wt%), followed by K₂O (~0.20 wt%) and P₂O₅ (~0.20 wt%). Ni among the transition group of elements shows maximum variation (~150 ppm), followed by Cr (~125 ppm) and Co (~100 ppm) (Fig. 6). Two distinct subparallel trends for Cr with #Mg probably suggest two different fractional crystallisation trends in NCIR basalts. The incompatible trace elements Zr shows maximum variations (~80 ppm), followed by Sr (~50 ppm) and Y (~25 ppm) (Fig. 6). The nearly flat REE pattern [(Ce/Yb)_N = 0.67–1.37] of the NCIR basalts (Fig. 7) suggest that these trace elements did not suffer any major fractionation during fractional crystallization of NCIR parent magma, except for a progressive enrichment during fractionation (Figs. 7 d,e,f).

3. 5. Composition of parental magma of NCIR basalts

It has been noted that the NCIR basalts show mixed incompatible trace element characters. Incompatible element ratios are highly variable in nature, extending from the values typical of depleted (N-type) MORB, e.g. Zr/Nb>30, (La/Sm)_N<1, to values characteristic of geochemically enriched (E-type) MORB, e.g. Zr/Nb<16, (La/Sm)_N>1 (Schilling 1975, Sun et al., 1979, le Roex et al., 1983). Transitional type (T-type) MORBs are classified as those rocks which have intermediate incompatible trace element characters. The VM and VT basalts with Zr/Nb=9.5-61, Zr/Y=2.7-3.8, Y/Nb=2.5-23 and K/Ti=0.03-0.74 dominate in three locations of the present study area and could be classified as N-type to T-type MORBs. In the chondrite normalised REE spiderdiagrams, the mixed magma character of the NCIR basalts are also clearly depicted (Fig. 7). The marginally depleted LREE character of the VT 4 basalt is similar to N-MORB, whereas no depletion or marginally enriched LREE pattern of the VT 5 and VM 9DG basalts reflect E-MORB character (cf. Sun and McDonough, 1989; Thompson et al., 1986).

Incompatible element ratios describe remarkably good mutual correlations in all samples analysed confirming the compositional variability within the present study area is controlled largely by mixing between geochemically depleted and enriched end member components. A Nb negative anomaly in many samples is clearly evident, suggesting the asthenospheric mantle beneath the NCIR is depleted to Nb compared to normal MORB mantle. The present observations, therefore, suggest that the NCIR basalts, in general, evolved by fractional crystallization of a parent magma, which shows mixed characters, either enriched with incompatible trace elements (e.g. Ba and Rb) or similar to depleted

normal MORB. The difference in the incompatible trace elements including REE suggest their difference in primary compositional characteristics. However, the parent magma for VM basalts seems to be more fertile than that of VT basalts.

3.6. Physical conditions of magma generation

Among the 83 major oxide analyses of the NCIR basalt (Table 4), 6% displays #Mg between 0.69 and 0.73. Presence of megacrystic plagioclase as porphyries within these high #Mg basalts (SO 28 cruise report; Pluger et al., 1988) suggests that they are not cumulate phases produced during fractionation of original parent magma, but represent primary MORB (#Mg > 0.68), which were generated by partial melting of mantle peridotite and did not suffer any significant change in composition after its segregation from mantle source (Hess, 1992). Among the five primitive magma compositions of the NCIR samples, 33 DR 01/2 is the most primitive member (#Mg = 0.73) and it is compositionally similar to one of the primitive ocean floor basalt of Presnall and Hoover (1987; Table 4, Fig. 3d).

Plot of the five primitive NCIR basalts in the normative olivine-diopside-silica diagram projected from plagioclase apex (after Walker et al., 1979, Fig. 8) shows that three of them are plotted very close to the 10 kbar ternary eutectic, while the others plot a little away from this eutectic and display a close affinity towards 15 kbar ternary eutectic. However, pressure of primary NCIR magma generation >10 kbar is unrealistic because most of the primitive members of the NCIR basalts contain plagioclase phenocryst, a mineral phase which is stable only at pressure \leq 10 kbar (Yoder and Tilley, 1962). Therefore, these two samples along with other three samples form a cluster around 10 kbar ternary eutectic.

Most of the evolved NCIR basalts, having #Mg < 0.68, plot on a linear trend, which is parallel to the 10 kbar cotectic line with decreasing temperature, but is skewed towards the diopside end (Fig. 8). It indicates that the evolved NCIR basalts were crystallised at < 10 kbar pressure. Direction of liquid line of descent towards the olivine-diopside join indicates that their crystallisation pressure should be greater than 5 kbar (Hess, 1992). Therefore, the pressure of crystallisation of the NCIR basalts was between 10 and 5 kbar. The NCIR basalts do not contain any primary amphibole in its mineralogy, which indicates low H₂O content of the peridotite source.

4. Discussion on petrogenesis of NCIR basalt

The NCIR basalts between 3° and 11°S are olivine tholeiite (predominance of only normative olivine; mean ~10.5, range ~0-22%) and a very poor presence of normative quartz

(0.02, 0-1.5%), which are similar to type-II IORB of Natland (1991) and grading to type- III in composition. Thus, the NCIR basalts are T-MORB in nature and appear to have been generated by partial melting of enriched mantle peridotite. In addition, published isotope data from the CIR show an increase in $^{87}\text{Sr}/^{86}\text{Sr}$ ratio (0.7031 to 0.7034) along with decrease in ϵNd (+ 7.0 to +7.9), accompanied by enrichments in incompatible elements (Murton, et al., 2005; Nauret et al., 2006), and these findings also corroborate with our geochemical observations.

A few NCIR basalts (n=5) show porphyritic texture (presence of megacryst of plagioclase and clinopyroxene not as cumulate phases generated due to fractionation of parent magma; Pluger et al., 1988) and have $\#Mg > 0.68$, suggesting their primary MORB nature. In the Di-Ol-Qz ternary plot (after Walker et al., 1979; Hess, 1992) of primitive NCIR basalts it is observed that they were generated at pressure ~ 10 kbar (Fig. 8), while the bulk of the fractionated basalts were crystallized within a pressure range of ~ 10 to 5 kbar.

During fractionation, the NCIR magma was systematically depleted in MgO and enriched in FeO_t , TiO_2 , P_2O_5 and Na_2O (Fig. 5). There was, however, very limited gradual depletion in Al_2O_3 and CaO, and less systematic enrichment in K_2O . Among the trace elements, the NCIR basalts are progressively enriched in Y and Zr and to some extent in Sr, and depleted in Ni and Cr during fractionation (Fig. 6).

The phenocryst population of the NCIR basalt consists of three silicate mineral phases, i.e. mostly calcic plagioclase ($\text{An}_{62-90} \leq 19$ vol %), less abundant forsteritic olivine (Fo_{81-88} , 0.04-1.69 vol%) and very rare diopside (≤ 0.05 vol%). One or all of these phenocrystic minerals might be the dominant phase(s) in the cumulate assemblage during fractionation of its parent magma. It is understood that major withdrawal of calcic plagioclase phenocryst in the cumulate phase would make the residual liquid relatively depleted in Al_2O_3 , CaO and Na_2O and enriched in TiO_2 , FeO_t , MnO, MgO and K_2O , while SiO_2 would remain unchanged. If it is only clinopyroxene, the residual liquid would be depleted mostly in TiO_2 and CaO, and enriched in Al_2O_3 , Na_2O and partly in K_2O , while SiO_2 , FeO_t and MgO will not change in proportions due to fractionation. In the present scenario, among the evolved NCIR basalts, none of the above chemical signatures are reflected. Thus, it is apparently clear that calcic plagioclase or diopside phenocrysts could not be the dominating cumulate phases in these rocks.

In the NCIR basalts, Sr shows an enrichment trend with decreasing $\#Mg$ (Fig. 6c). Plagioclase feldspar could be a potential source for Sr [Partition coefficient, K_{Sr} for

plagioclase in basaltic liquid is 1.83; cf. Rollinson, 1993). Fractionation of plagioclase from the crystallising liquid, therefore, would make the residual liquid depleted in Sr. Hence the observed higher enrichment trend of Sr also rules out the possibility of plagioclase being a dominating cumulate phase during fractionation of NCIR mother magma.

A similar explanation can also be substantiated by REE pattern of the NCIR basalt (Fig. 7). If plagioclase is the dominating cumulate phase, the evolved NCIR basalt should show negative Eu anomaly due to major withdrawal of Eu from the melt by plagioclase. Fractionated REE pattern [i.e. $(La/Yb)_N > 1$] may also have resulted if there was a major withdrawal of HREE by clinopyroxene cumulates during fractionation (Rollinson, 1993). However, none of these REE patterns are shown by the NCIR basalts (Fig. 7) and hence, the probability of early crystallization of calcic plagioclase or diopside as major cumulate phases from the parent NCIR melt is ruled out. Furthermore, a flat HREE $(Gd/Yb)_N$ pattern of the NCIR basalts also eliminates the possibility of major crystallization of HREE bearing other major mafic silicates (e.g. orthopyroxene, garnet, cf. Rollinson, 1993) from the NCIR parent magma.

Therefore, withdrawal of olivine as a major cumulate phase from the NCIR parent magma is the best remaining possibility, which would make the residual liquid relatively enriched in FeO_T over MgO. Major withdrawal of olivine would additionally make the residual liquid enriched in TiO_2 , Na_2O and K_2O , and marginally in SiO_2 , which are, in fact, observed for the NCIR magma (Fig. 5). However, a disparity rises while considering only olivine as the major cumulate phase withdrawn from the NCIR parent magma. Withdrawal of olivine would make the residual liquid relatively enriched in Al_2O_3 and CaO, which are not seen at all in the bulk compositions of the NCIR basalts (Fig. 6). The NCIR magma is marginally depleted in Al_2O_3 (~3 wt%) and CaO (~2 wt%) with decreasing #Mg (Fig. 5).

On the other hand, although Rollinson (1993) reaffirmed that early withdrawal of olivine likely make the residual liquid depleted mostly in Ni, Co and Mn and very little in Cr, the fractionating NCIR magma does not show this chemistry. In stead, it shows no change in MnO, strong depletion in Cr and Ni (Fig. 6). Therefore, early crystallization of only olivine from the NCIR parent magma as cumulate doesn't satisfy the model. To model the major depletion of Mg, Ni and Cr in the evolved NCIR basalts (Fig. 6) along with its flat REE pattern (Fig. 7), we propose early crystallization of spinel from the NCIR parent magma during its first phase of fractional crystallisation. As this mineral is a major source of Al_2O_3 , crystallization of this mineral would make the residual NCIR magma depleted in Al_2O_3 . The

trace elements, Cr and Ni, both are also withdrawn from the basaltic parent liquid in addition to Mg during early crystallisation of spinel ($K_{Cr \text{ and } Ni}$ for spinel in basaltic liquid are 10 and 5 respectively, Cox et al., 1979, p. 334). When the ascending magma crossed the ~10 kbar pressure domain, spinel ceased to crystallize and olivine took its place. The crystallisation of olivine made the residual liquid again enriched in Al_2O_3 and the marginally depleted slope for this oxide finally resulted for NCIR magma (Fig. 5c). The crystallization of spinel and olivine does not incorporate any HREE during their crystallization (Olivine, of course, incorporate negligible proportion of HREE, cf. White, 1999, p. 281; Rollinson, 1993), and hence a flat REE pattern of the NCIR magma has been resulted.

Though olivine withdraws a major proportion of Co, along with Ni and minor Mn, during its crystallization from basaltic magma, the NCIR magma does not show any depletion of this element during fractionation (Fig. 6d). As Co shows replacement relationship with Mg in olivine structure (Mason, 1958), we propose crystallization of relatively Fe rich olivine cumulate from the NCIR parent magma. In fact, our microprobe data shows that the olivine phenocrysts of the NCIR magma are relatively Fe rich and they contain ~0.5 time Fe to that of Mg (Table 2). The Fe-rich olivine also incorporates some CaO [cf. Deer et al., 1992, Table 2] and hence, early crystallization of Fe-rich olivine from the NCIR parent magma made the residual liquid marginally depleted in CaO (Fig. 5e).

5. Conclusions

- (1) The NCIR basalts between 3^0 and 11^0S latitudes are enriched in highly incompatible elements, and can be classified as olivine basalts, that appear to have been generated from an enriched mantle peridotite.
- (2) Comparison with experimental phase diagrams shows that the primitive NCIR MORB, having $\#Mg > 0.68$, were generated by partial melting of mantle peridotite at a pressure ~10 kbar.
- (3) The parent NCIR magma was modified by fractional crystallization when spinel separated from the melt in the first phase at pressure >10 kbar and was followed by fractionation of Fe-rich olivine at pressure <10 kbar. The bulk of the NCIR daughter magma crystallized within a pressure range of ~10 to 5 kbar.
- (4) Fractionation is the most possible process that would have influenced the compositional characteristic of NCIR MORBs during its evolution. During fractionation, the magma was systematically depleted in MgO and enriched in FeO_t ,

TiO₂, P₂O₅ and Na₂O. There was, however, a very limited gradual depletion in Al₂O₃ and CaO, and enrichment in K₂O.

Among the trace elements, the NCIR basalts were depleted in Ni and Cr and progressively enriched in Y and Zr and to some extent in Sr during fractionation. Total REE of the NCIR magma increased with fractionation but there is no change in REE slope (La/Yb)_N, particularly that of HREE (Gd/Yb)_N, with progressive evolution of the NCIR basalt.

Acknowledgement

We thank Director, NIO, for permission to publish the manuscript. We are grateful to Dr. V. Balaram (Head, Geochemistry Division, NGRI, Hyderabad) for analytical support (ICP-MS). We acknowledge the Department of Geology, Presidency College, Kolkata, Department of Geology & Geophysics, Indian Institute of Technology, Kharagpur and SEM-EDS lab, NIO (Mr. V.D. Khedekar) for rendering assistance in many ways. We thank the Department of Ocean development, New Delhi for the availability of ORV Sagar Kanya and National Centre for Antarctic and Ocean Research (NCAOR), Goa, for allotting the cruise as scheduled and for the logistics. We acknowledge the scientific party and crew of ORV Sagar Kanya, Cruises 125 and 165, during sample collection. D.R. gratefully acknowledges the support of CSIR-Senior Research Fellowship. This work was supported largely by ONR, USA (grant# 00144-97-1-0925). S.M. is grateful to CSIR, New Delhi, for providing him a financial support through their Senior Research Associateship (SRA) scheme (grant no. B-10220) for this work. First author (D.R.) is thankful to Prof. Somnath Dasgupta of Jadavpur University, Kolkata for his constructive comments. We thank Dr. Yusheng Wan for his critical comments and suggestions to improve the manuscript. This is NIO's contribution #.....

References:

- Balaram, V., Gnaneshwara Rao, T., and Anjaiah, K.V., 1999, International proficiency tests for analytical geochemistry laboratories: an assessment of accuracy and precision in routine geochemical analysis. *J. Geol. Soc. India*, 53: 417-423.
- Banerjee, R., and Iyer, S.D., 1991. Petrography and chemistry of basalts from the Carlsberg Ridge. *J. Geol. Soc. India*, 38: 369-386.
- Banerjee, R., and Iyer, S.D., 2003. Genetic aspects of basalts from the Carlsberg Ridge. *Current Sci.*, 85 (3): 299-305.
- Bougalt, H., and Hekinian, R., 1974. Rift valley in the Atlantic Ocean near 36°50'N: petrology and geochemistry of basaltic rocks. *Earth and Planet. Sci. Lett.*, 24: 249-261.
- Cann, J.R., and Vine, F.J., 1967. An area on the crest of the Carlsberg Ridge; petrologic and magnetic survey. *Phil. Trans. of Royal Soc. of London*, 259: A198-A298.
- Cohen, R.S., Evensen, N.M., Hamilton, P.J., and O'Nions, R.K., 1980. U-Pb, Sm-Nd and Rb-Sr systematics of mid-ocean ridge basalt glasses. *Nature*, 283: 149-153.
- Cox, K. G., Bell, J. D., and Pankhurst, R. J., 1979. The interpretation of igneous rocks: London, George Allen and Unwin, 450p.
- David, K., Schiano, P., and Allegre, C.J., 2000. Assessment of the Zr/Hf fractionation in the oceanic basalts and continental materials during petrogenetic processes. *Earth and Planet. Sci. Lett.*, 178, 285-301.
- Deer, W.A., Howie, R.A., and Zussman, J., 1992. An introduction to the rock-forming minerals: Essex, ELBS, 696 p.
- Droliia, R.K., Ghose, I., Subrahmanyam, A.S., Malleswara Rao, M.M., Kessarkar, P., and Murthy, K.S.R., 2000. Magnetic and bathymetric investigations over the Vema regions of the Central Indian Ridge: Tectonic implications. *Mar. Geol.*, 167, 413-423.
- Droliia, R. K., Iyer, S.D., Chakraborty, B., Kodagali, V., Ray, D. Misra, S. Andrade, R., Sarma, K.V.L.N.S., Rajasekhar, R.P., and Mukhopadhyay, R., 2003. The Northern Central Indian Ridge: Geology and tectonics of fracture zones-dominated spreading ridge segments. *Current Sci.*, 85 (3), 290-298.
- Engel, C.G., and Fisher, R.L., 1975. Granitic to ultramafic rock complexes of the Indian ocean ridge system, Western Indian Ocean. *Bull. Geol. Soc. America*, 82, 553-562.
- Hekinian, R., 1968. Rocks from the mid-ocean ridge in the Indian Ocean: *Deep-Sea Res.*, 15, 195-213.
- Hellebrand, E., Snow, J.E., Hoppe, P., and Hofmann, A.W., 2002. Garnet-field melting and late-stage refertilisation in 'residual' abyssal peridotites from the Central Indian Ridge. *J. Petrology*, 43, 2305-2338.

- Herzig, P.M., and Pluger, W.L., 1988. Exploration for hydrothermal activity near the Rodriguez Triple Junction, Indian Ocean. *Can. Mineral.*, 26, 721-736.
- Hess, P.C., 1992. Phase equilibria constraints on the origin of Ocean Floor basalts: In Morgan, J.P., Blackman, D.K. and Sinton, J.M. (eds). *Mantle flow and melt generation at Mid-Ocean ridges*, Geophysical Monograph, American Geophysical Union, 67-102.
- Humler, E., and Whitechurch, H., 1988. Petrology of basalts from the Central Indian Ridge (lat 25°23'S, long. 70°04'E): estimates of frequencies and fractional volumes of magma injections in a two-layered reservoir. *Earth and Planet. Sci. Lett.*, 88, 169-181.
- Ito, E., White, W.M., and Gopel, C., 1987. The O, Sr, Nd and Pb geochemistry of mid-ocean ridge basalt. *Chem. Geol.*, 62, 157-176.
- Iyer, S.D., and Banerjee, R., 1993. Mineral chemistry of Carlsberg Ridge basalts. *Geo-Mar. Lett.*, 13, 153-158.
- le Roex, A.P., Dick, H.J.B., Earlanck, A.J., Reid, A.M., Frey, F.A., Hart, S.R., 1983. Geochemistry, mineralogy and paragenesis of lavas erupted along the Southwest Indian Ridge between the Bouvet triple junction and 11 degrees east. *J Petrol.*, 24, 267-318.
- McDonough, W.F., and Sun, S.S., 1995. The composition of the Earth, *Chem. Geol.*, 120, 223-253.
- Mason, B., 1958. Principles of geochemistry (2nd Ed.): New York, Wiley International, 310p.
- Melson, W.G., and O'Hearn, T. 1976, Smithsonian Volcanic Glass File
- Michard, A., Monigny, R., and Schlich, R., 1986. Geochemistry of the mantle beneath the Rodriguez triple Junction and South-east Indian ridge. *Earth and Planet. Sci. Lett.*, 78, 104-111.
- Mudholkar, A. V., 2001, Magmatic evolution of the fresh basalts from the ridge axis near Egeria fracture zone. *J. Geol. Soc. India*, 58, 329-339.
- Mukhopadhyay, R., Murthy, K.S.R., Iyer, S.D., Melleswara Rao, M.M., Banerjee, R., Subramanyam, A.S., Shirodkar, P.V., and Ghose, I., 1998. InRidge Program: Preliminary results from the first cruise. *Current Sci.*, 75, 1157-1161.
- Murton, B.J., Tindle, A.G., Nilton, J.A., and Sauter, D., 2005. Heterogeneity in southern Central Indian Ridge MORB: Implications for ridge-hotspot interaction. *Geochemistry Geophysics Geosystems*, doi 10.1029/2004GC000798.
- Natland, J.H., 1991. Indian Ocean crust. In: Floyd, P.A. (ed.), *Oceanic Basalts*, Blackie and Sons, Glasgow, 289-310.
- Nauret, F., Abouchami, W., Galer, S.J.G., Hofmann, A.W., Hemond, C., Chauvel, C. and Dyment, J., 2006. Correlated trace elemnt-Pb isotope enrichments in Indian MORB along 18-20°S, Central Indian ridge, *Earth and Planet. Sci. Lett.*, 245, 137-152.

- Petrological Database of Ocean floor, website: <http://beta.petdb.ciesin.columbia.edu/index.jsp>
- Pluger, W.L. and all cruise participants, 1988. Fahrtbericht SO 28 and Wissenschaftlicher Bericht GEMINO I: Geothermal Metallogenesis Indian Ocean.
- Presnall, D.C., and Hoover, J.D., 1987. High pressure phase equilibrium constraints on the origin of mid-ocean ridge basalts. In: Mysen, B.O. (ed.), *Magmatic Processes: Physicochemical principles*, Geochemical Society Special Publication, London, 1, 75-89.
- Price, R.C., Kennedy, A.K., Riggs-Sneeringer, M., and Frey, F.A., 1986. Geochemistry of basalts from the Indian ocean triple junction: implications for the generation and evolution of Indian Ocean ridge basalts. *Earth and Planet. Sci. Lett.*, 78, 379-396.
- Rehkamper, M., and Hoffman, A.W., 1997. Recycled ocean crust and sediment in Indian Ocean MORB. *Earth and Planet. Sci. Lett.*, 147, 93-106.
- Rollinson, H. R., 1993. Using geochemical data: Evaluation, presentation, interpretation. Longman, England, 352 p.
- Schiano, P., Birck, J.L., and Allegre, C.J., 1997. Os-Sr-Nd-Pb isotopic covariations of mid-ocean ridge basalt glasses and heterogeneity of the upper mantle. *Earth and Planet. Sci. Lett.*, 150, 363-379.
- Schilling, J.G., Zajac, M., Evans, R., Johnson, T., White, W.M., Devine, J.D. and Kingsley, R., 1983. Petrologic and geochemical variations along the Mid-Atlantic Ridge from 29° to 73°N, *Am. J. Sci.*, 283, 510-586.
- Subbarao, K.V., and Hedge, C.E., 1973. K, Rb, Sr and ⁸⁷Sr/⁸⁶Sr in rocks from the Mid-Indian Ocean Ridge. *Earth and Planet. Sci. Lett.*, 18, 223-228.
- Sun, S.S., Nesbitt, R.W., and Sharaskin, A.Y., 1979. Geochemical characteristics of mid-ocean ridge basalts. *Earth and Planet. Sci. Lett.*, 44, 119-138.
- Sun, S.S., and McDonough, W.F., 1989. Chemical and isotope systematics of ocean basalts: implications for mantle composition and processes. In: Saunders, A.D. and Norry, M.J. (eds.), *Magmatism in the Ocean Basins*. Geological Society of London Special Publication, London, 42, 313-345.
- Thompson, R.N., Morrison, M.A., Dickin, A.P., Gibson, I.L., and Harmon, R.S., 1986. Two contrasting styles of interaction between basic magmas and continental crust in the British tertiary volcanic province. *J. Geophys. Res.*, 91, 5985-97.
- Walker, D., Shibata, T., and DeLong, S.E., 1979. Abyssal tholeiites from the Oceanographer fracture zone, II: Phase equilibria and mixing. *Contrib. Mineral. Petrol.*, 70, 111-125.
- White, W. M., 1999. Trace elements in igneous processes, In: Dasch E. J. (ed.) *Encyclopedia of Earth Sciences*, Macmillan, U.S.A., 1, 256-307.
- Yoder, H.S., and Tilley, C.E., 1962. Origin of basalt magmas: an experimental study of natural and synthetic rock system. *J. Petrol.*, 3, 342-532.

About the first Author

Dwijesh Ray, Male, Born in 1975; Senior Research Fellow (Council of Scientific and Industrial Research, INDIA), presently pursuing doctoral research on the problem “Spreading Ridge Kinematics and petrological characters of rocks from Northern Central Indian Ridge, Indian Ocean.” His research is primarily focused on understanding magmatic and geochemical processes beneath the oceanic ridge system by studying the MORB geochemistry (both mineral and whole-rock geochemistry), low temperature geochemistry (seawater-rock interaction with special emphasis on serpentine chemistry) and seafloor hydrothermal processes. He is presently student member of American Geophysical Union and The Geochemical Society.

Table captions

Table 1. Geographic position and depth of sample locations in NCIR.

Table 2. Average chemical composition of mineral phases in NCIR basalt.

Table 3. Representative major and trace element analyses of NCIR basalt samples. For sample locations see Fig. 1.

Table 4. Comparison of average major element compositions of NCIR basalts with other Indian Ocean Ridge Basalts (IORB).

Table 1

Station	Lat (S)	Long (E)	Depth (m)	Tectonic setting
VT 4	5°39.06'	68°03.8'	3050	Outer ridge flank
VT 5	5°35.2'	67°54.9'	3560	Outer ridge flank
VM 9 DG	9°53.64'	66°35.7'	2000	Near axis seamount (summit height 1875 m), west of ridge segment # 3

Table 2

	Plagioclase			Olivine			Clinopyroxene			Titanomagnetite		
	VT	VM	VM	VT	VM	VM	VM	VM	VM	VM	VM	VM
No. of grains	7	6	6	6	3	6	6	6	7	7	7	7
No. of analyses	21	18	18	18	9	18	18	18	21	21	21	21
SiO ₂	average 50.92	average 51.95	range 47.91-56.32	average 41.31	average 40.67	range 40.46-41.94	average 45.51	average 45.51	range 42.09-48.11	average 2.74	average 2.74	range 0.89-6.6
TiO ₂	0.22	0.10	0.03-0.18	0.03	0.03	0.01-0.08	2.70	2.70	1.9-3.29	22.69	22.69	18.17-38.53
Al ₂ O ₃	28.69	28.30	25.4-32.02	0.18	0.05	0.01-0.85	8.09	8.09	4.18-13.41	1.67	1.67	0.72-2.64
FeOt	1.02	0.67	0.2-1.09	14.02	11.64	12.43-17.26	10.41	10.41	7.85-12.01	63.75	63.75	42.9-69.57
CaO	15.02	13.75	10.28-17.58	0.34	0.2	0.27-0.4	21.66	21.66	19.88-23.22	0.46	0.46	0.25-0.88
MgO	0.34	0.30	0.12-0.54	43.45	44.49	41.22-45.01	10.24	10.24	6.95-12	0.94	0.94	0.8-1.09
MnO	0.08	0.07	0.03-0.13	n.d.	0.32	-	0.22	0.22	0.15-0.3	0.63	0.63	0.48-0.74
Na ₂ O	2.76	3.33	1.68-5.21	n.d.	0.01	-	0.43	0.43	0.32-0.75	1.17	1.17	-
K ₂ O	0.04	0.07	0.03-0.13	0.03	0.04	-	0.03	0.03	0.01-0.04	n.d.	n.d.	-
Cr ₂ O ₃	0.03	0.11	-	0.06	0.11	0.03-0.1	0.12	0.12	0.07-0.17	0.52	0.52	-
Total	99.06	98.51	-	99.39	97.50	-	99.30	99.30	-	94.72	94.72	-
An	74.75	69.17	51.91-85.2	84.65	87.19	80.96-86.57	Wo	49.25	45.49-51.07			
Ab	25.04	30.44	14.71-47.68	15.34	12.81	13.43-19.04	En	32.16	24.84-36.98			
Or	0.22	0.39	0.1-0.93				Fs	18.59	13.57-24.10			

n.d. not detected

Table 3

	VT 4/2	VT 4/3	VT 4/4	VT 4/5	VT 4/N1*	VT 4/N2*	VT 5/6A3	VT 5/6A4	VT 5/6B	VM7A	VM1B	VM4A	VM4B	VM5B	VM6A	WS-E and OUG 9**	MO 12 and W2	JB 2
Major (wt%)																		
SiO ₂	49.52	50.10	49.33	48.91	50.11	49.16	49.99	49.96	50.01	52.17	49.25	49.83	49.08	49.50	47.27	±1	±5	
TiO ₂	1.66	1.73	1.14	1.65	1.22	1.17	1.34	1.52	1.55	1.84	1.66	1.15	1.38	1.69	1.15	±1	±5	
Al ₂ O ₃	15.32	16.02	16.43	15.57	16.82	16.18	16.37	15.03	15.17	15.31	15.97	17.93	16.41	15.72	17.64	±1	±5	
FeO _x	10.01	10.36	8.56	10.62	8.56	8.66	8.88	9.68	9.74	8.34	9.54	7.62	8.51	9.56	8.17	±1	±5	
MnO	0.16	0.19	0.16	0.25	0.14	0.14	0.37	0.17	0.16	0.25	0.19	0.14	0.18	0.18	0.51	±1	±5	
MgO	6.26	6.79	8.61	6.33	9.06	8.39	7.57	6.92	7.08	7.63	6.35	7.48	7.00	6.61	6.07	±1	±5	
CaO	10.94	11.22	11.51	10.94	11.72	11.47	11.50	11.02	10.95	10.49	10.31	11.48	10.74	10.53	10.59	±1	±5	
Na ₂ O	2.72	2.91	2.86	2.81	2.92	2.73	3.01	3.18	3.18	2.92	3.12	3.05	3.06	3.27	3.63	±1	±5	
K ₂ O	0.47	0.17	0.10	0.37	0.03	0.05	0.27	0.33	0.26	0.35	0.52	0.47	0.40	0.26	0.77	±1	±5	
P ₂ O ₅	0.16	0.17	0.09	0.18	0.09	0.08	0.14	0.19	0.18	0.19	0.21	0.18	0.19	0.21	0.25	±1	±5	
LOI	n.d.	n.d.	n.d.	0.38	n.d.	n.d.	n.d.	n.d.	n.d.	n.d.	0.88	0.72	0.63	0.95	1.27	±1	±5	
Total	97.22	99.66	98.79	98.01	100.67	98.03	99.44	98	98.28	99.49	97.35	100.05	97.58	98.48	97.32			
#Mg	0.53	0.54	0.64	0.52	0.65	0.63	0.60	0.56	0.57	0.59	0.54	0.64	0.60	0.55	0.57			
Na ₂ O+K ₂ O	3.19	3.08	2.96	3.18	2.95	2.78	3.28	3.51	3.44	3.27	3.64	3.52	3.46	3.53	4.40			
K ₂ O/Na ₂ O	0.17	0.06	0.03	0.13	0.01	0.02	0.09	0.10	0.08	0.12	0.17	0.15	0.13	0.08	0.21			
CaO/Al ₂ O ₃	0.71	0.70	0.70	0.70	0.70	0.71	0.70	0.73	0.72	0.66	0.67	0.64	0.65	0.67	0.60			
Al ₂ O ₃ /TiO ₂	9.23	9.26	14.41	9.44	13.79	13.83	12.22	9.89	9.79	8.7	9.21	15.58	11.87	9.30	15.35			
Trace (ppm)																		
Sc	37.92	38.30	36.23	37.85	36.06	36.42	37.38	37.10	36.80	37.56	35.91	31.60	32.89	36.12	32.16			+0.05/-2
V	301.12	309.06	247.96	302.51	247.93	253.04	275.03	276.98	280.35	302.31	295.71	235.86	265.93	302.1	251.99			+0.05/-2
Cr	235.46	231.9	329.18	234.39	332.34	329.23	331.06	293.10	302.24	225.52	215.43	238.18	222.93	217.81	191.27			+0.05/-3
Co	69.04	95.07	68.76	60.58	78.47	126.51	58.96	71.32	60.39	140.02	133.65	102.66	134.69	112	217.07			+0.05/-2
Ni	97.83	87.19	139.13	96.87	137.62	134.64	100.54	107.36	110.41	83.20	70.03	104.04	90.35	71.09	133.17			+0.05/-2
Cu	77.49	78.83	89.25	103.53	89.74	90.07	84.06	78.30	81.28	77.5	65.22	80.61	79.94	69.36	122.86			+0.05/-2
Zn	127.9	133.7	112.94	131.60	96.08	99.84	111.67	122.13	125.17	139.03	145.33	89.82	111.29	131.32	97.74			+0.05/-2
Ga	17.61	17.52	15.67	17.05	16.11	16.57	17.08	17.77	17.45	18.57	16.77	13.13	15.65	16.79	16.62			+0.05/-2
Rb	10.49	1.98	1.60	7.53	0.53	1.03	3.57	5.88	5.32	5.24	9.66	6.27	5.85	3.45	21.22			+0.05/-2
Sr	118.45	121.13	112.22	127.60	107.21	108.99	158.55	148.30	140.43	134.46	136.2	160.55	146.01	136.75	227.52			+0.05/-2
Y	44.58	45.04	29.99	44.22	29.38	30.63	34.07	41.94	42.31	42.49	42.07	26.7	34.28	43.19	29.95			+0.05/-2
Zr	132.60	134.94	80.75	134.63	78.38	81.24	109.49	140.9	143.09	146.35	135.95	88.88	116.43	140.97	114.43			+0.05/-2
Nb	2.97	3.06	1.31	3.11	1.29	1.62	3.53	4.08	4.26	6.13	5.76	6.14	5.63	5.59	12.06			-4/-7
Cs	0.67	0.04	0.03	0.42	0.01	0.05	0.17	0.43	0.38	0.08	0.48	0.13	0.13	1.22				-2
Ba	23.84	27.29	16.89	30.91	9.98	13.64	31.56	35.36	36.26	45.93	43.71	79.5	67.13	45.65	173.57			-1

La	4.43	4.47	2.48	5.59	2.07	2.24	4.64	5.21	6.01	5.46	6.19	4.38	5.27	6.21	11.65			±5
Ce	13.98	14.80	8.28	16.86	7.31	7.68	13.18	15.8	17.01	15.84	17.22	11.23	14.84	16.69	27.39			±5
Pr	2.04	2.06	1.27	2.23	1.13	1.20	1.79	2.21	2.36	2.17	2.34	1.45	1.93	2.37	2.63			±5
Nd	13.53	14.07	8.61	14.44	8.26	8.72	11.91	14.99	15.69	14.40	14.9	9.39	12.25	15.11	15.4			±5
Sm	4.38	4.46	2.94	4.52	2.78	2.94	3.62	4.44	4.56	4.28	4.51	2.73	3.72	4.65	3.83			±5
Eu	1.5	1.57	1.14	1.58	1.11	1.12	1.38	1.57	1.67	1.52	1.53	1.05	1.34	1.56	1.36			±5
Gd	6.38	6.56	4.32	6.57	4.15	4.30	5.19	6.33	6.45	6.14	6.39	3.97	5.32	6.56	5.25			±5
Tb	1.17	1.19	0.79	1.21	0.77	0.80	0.92	1.14	1.15	1.12	1.16	0.70	0.95	1.17	0.88			±5
Dy	6.75	6.91	4.6	6.86	4.48	4.68	5.36	6.44	6.56	6.42	6.58	4.02	5.47	6.74	4.83			±5
Ho	1.46	1.5	1.01	1.50	0.96	1.02	1.14	1.38	1.42	1.37	1.44	0.88	1.19	0.46	1.02			±5
Er	4.68	4.74	3.17	4.76	3.07	3.22	3.58	4.37	4.46	4.37	4.5	2.8	3.69	4.61	3.21			±5
Tm	0.78	0.8	0.52	0.79	0.52	0.55	0.61	0.76	0.78	0.74	0.76	0.48	0.61	0.75	0.56			±5
Yb	4.22	4.24	2.84	4.18	2.86	3.02	3.27	4.07	4.08	4.01	3.99	2.55	3.34	4.16	2.95			±5
Lu	0.66	0.68	0.45	0.67	0.42	0.45	0.49	0.59	0.61	0.60	0.64	0.38	0.53	0.65	0.44			±5
Hf	3.19	3.23	2.02	3.22	1.93	1.95	2.56	3.26	3.31	3.34	3.27	2.06	n.d.	3.41	n.d.			±5
U	0.10	0.09	0.14	0.15	0.05	0.06	0.12	0.13	0.18	0.12	0.14	0.11	0.13	0.15	0.4			±5
[La/Sm] _N	0.63	0.63	0.53	0.77	0.46	0.48	0.80	0.73	0.82	0.80	0.86	1.0	0.88	0.83	1.9			
[Ce/Yb] _N	0.87	0.92	0.77	1.06	0.67	0.67	1.06	1.02	1.10	1.04	1.13	1.16	1.17	1.05	2.44			

Total Fe calculated as FeO.

#Mg=mole [Mg/ (Mg+Fe)]

* Glassy basalts

** Accuracy in wt%

Table 4

	CR ^a		NCIR ^b				SCIR ^c		Primitive MORB ^d	
	Whole rock and glass (literature)	Whole rock and glass (literature)	VT glass and whole-rock	VM whole-rock	Least evolved member	Whole-rock and glass (literature)	Average composition	A primitive MORB composition		
N=	98	50	26	7	33 DR 01/2 ¹	137	48	525-53 ²		
SiO ₂	50.69 (0.82)	50.54 (0.85)	49.35 (1.45)	48.93 (0.84)	49.56	50.97 (0.19)	49.80 (1.19)	48.96		
TiO ₂	1.32 (0.27)	1.36 (0.32)	1.56 (0.22)	1.48 (0.24)	0.88	1.22 (0.77)	0.89 (0.63)	0.82		
Al ₂ O ₃	15.42 (0.63)	15.74 (0.67)	15.58 (0.95)	16.24 (1.13)	16.14	15.90 (0.50)	16.28 (0.96)	15.75		
FeO _T	9.79 (1.58)	9.36 (0.98)	10.11 (0.93)	8.81 (0.74)	7.72	8.98 (0.02)	8.18 (0.59)	8.44		
MnO	0.14 (0.04)	0.15 (0.02)	0.21 (0.09)	0.22 (0.13)	0.14	0.16 (0.58)	0.08 (0.07)	0.13		
MgO	7.80 (1.04)	8.17 (1.24)	7.43 (0.84)	6.58 (0.50)	11.59	7.93 (0.64)	10.03 (1.21)	9.79		
CaO	10.53 (1.42)	11.36 (0.73)	11.16 (0.42)	10.60 (0.43)	11.53	11.87 (0.27)	12.33 (0.80)	11.92		
Na ₂ O	3.16 (0.81)	2.74 (0.32)	2.87 (0.33)	3.20 (0.21)	2.13	2.52 (0.12)	2.11 (0.32)	1.97		
K ₂ O	0.47 (0.44)	0.11 (0.05)	0.24 (0.13)	0.46 (0.17)	0.11	0.14 (0.05)	0.08 (0.08)	0.11		
P ₂ O ₅	0.14 (0.04)	0.11 (0.05)	0.15 (0.03)	0.20 (0.02)	0.05	0.12 (0.03)				
#Mg	0.59 (0.05)	0.61 (0.05)	0.57 (0.04) ³	0.57 (0.03) ³	0.73	0.61 (0.04)	0.68 (0.02)	0.67		
CaO/Al ₂ O ₃	0.68 (0.11)	0.72 (0.06)	0.72 (0.03)	0.65 (0.03)	0.71	0.75 (2.69)	0.76 (0.06)	0.76		
Al ₂ O ₃ /TiO ₂	12.41 (3.90)	12.35 (3.30)	10.23 (2.05)	11.42 (2.92)	18.34	13.48 (0.35)	23.75 (25.26)	19.21		
K ₂ O/Na ₂ O	0.13 (0.10)	0.04 (0.02)	0.08 (0.05)	0.14 (0.05)	0.05	0.05 (0.01)	0.04 (0.04)	0.06		
K ₂ O+Na ₂ O	3.62 (1.21)	2.85 (0.33)	3.11 (0.38)	3.67 (0.33)	2.24	2.66 (0.04)	2.19 (0.34)	2.08		

^a Data sources: [Hekinian, 1968, Banerjee and Iyer, 1991, Rehkamper and Hofmann, 1997, Cann, and Vine, 1967, Melson and O'Hearn, 1976, Sun, et al., 1979, Cohen, et al., 1980, Ito et al., 1987]; ^b [Wiseman, 1937, Engel and Fisher, 1975, Melson and O'Hearn, 1976, Ito et al., 1987, and Plugger et al., 1988, Schiano, 1997, Rehkamper and Hofmann, 1997, David, 2000] and present study; ^c [Engel and Fisher, 1975, Melson and O'Hearn, 1976, Subbarao and Hedge, 1979, Michard et al., 1986, Herzog and Plugger, 1989, Natland, 1991, Plugger et al., 1988, Mahoney, 1989 and Mudholkar, 2001]; ^d [Presnall and Hoover, 1987]

#Mg [magnesian number, mole Mg/ mole (Mg+Fe)] values, ¹ One of the primitive MORB composition similar to least evolved member of NCIR basalt (33 DR 01/2, SO 28 cruise report), ² Primitive MORB composition from [Presnall and Hoover, 1987]

³ Range of #Mg values for VT basalts- 0.51 - 0.65, for VM basalts- 0.54 - 0.64.

Figure captions

Fig. 1. Generalised map of IORS shows three sample locations (VT 4, VT 5 and VM 9DG). CR~ Carlsberg Ridge, NCIR~ Northern Central Indian ridge, CIR~ Central Indian Ridge, RTJ~ Rodriguez Triple Junction, SWIR~ Southwest Indian Ridge and SEIR~ Southeast Indian Ridge. The smaller rectangle on the NCIR indicates the broad boundaries of the present study area. The precise three sample locations are shown in two enlarged maps (a. VT area and b. VM area). Depth contour map scale 1: 5000000.

Fig. 2. Photomicrographs of NCIR basalts: (a) Plagioclase phenocryst: One half showing twinning while the other half is zoned (VT 4/2, crossed nicol, objective 5X). Scale bar 0.4 mm. (b) String let of melt inclusions showing cleavage-parallel orientation (VM 3B, crossed nicol, objective 2X). Scale bar 1 mm.

Fig. 3 (a) Primitive MORB normalized spiderdiagram for major oxides and some ratios of NCIR basalts from literature. Average primitive MORB composition after Presnall and Hoover, 1987. The abbreviated parameters along the abscissa represent respective oxides and their ratios. (b) The same diagram for VT- and VM- basalts. (c) The same for average CR, NCIR, SCIR, VT- and VM- basalts (Table 4). (d) Primitive NCIR basalt (33 DR 01/2) normalized spiderdiagram showing variation between a primitive MORB sample (525-53, after Presnall and Hoover, 1987), average NCIR, VT-, VM basalts.

Fig. 4. Primitive mantle normalized trace element abundance patterns in MORB from NCIR. Panel a, b and c represent the VT 4, VT 5 and VM 9DG samples. Normalizing values from Sun and McDonough, 1989.

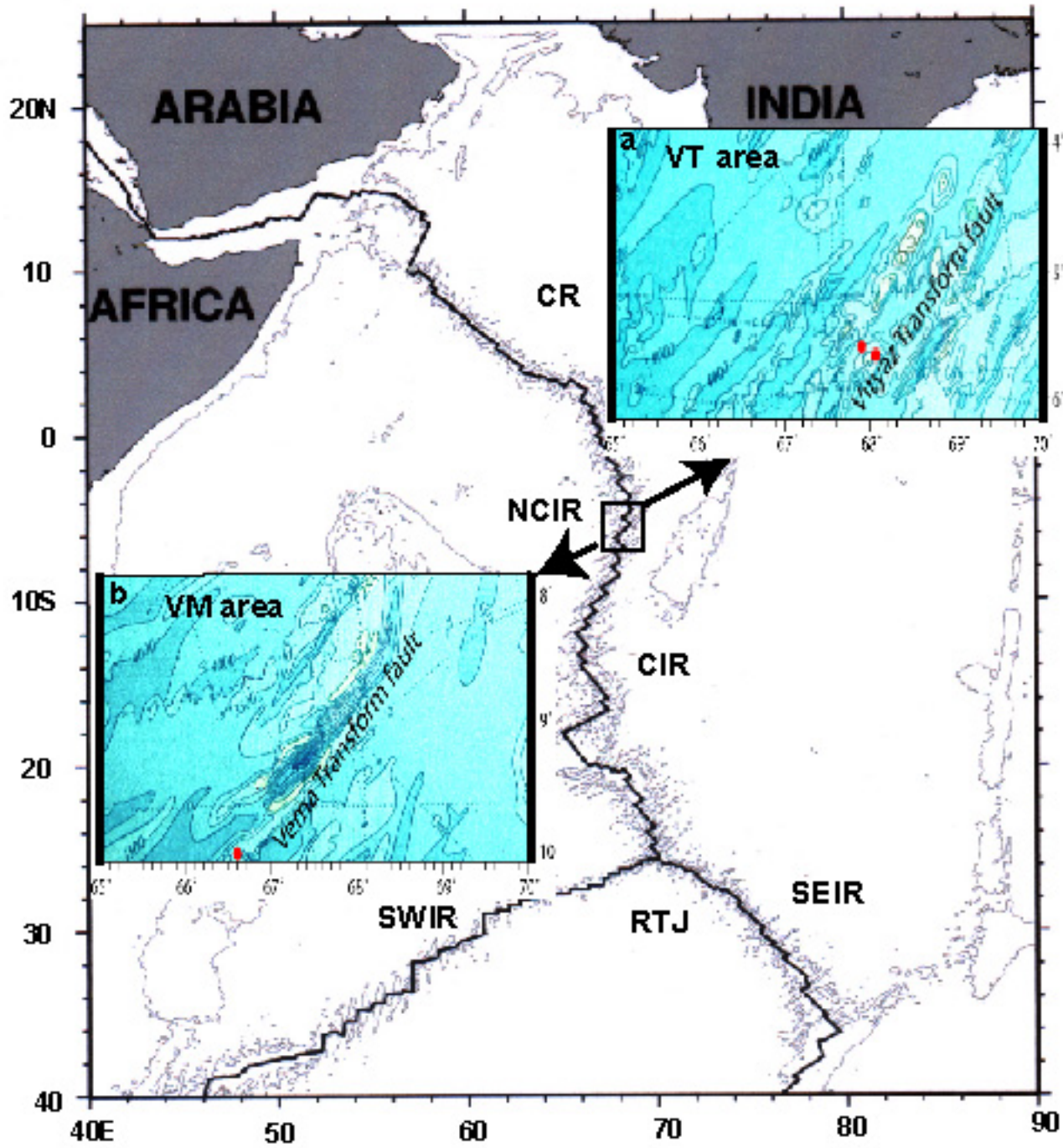
Fig. 5. (a) NCIR basalts in TiO_2 versus Na_2O plot, data as referred in Table 4 and present study. Type I, II, III Indian Ocean Ridge basalts (Natland, 1991); 5 (b-h) magnesian number (#Mg) versus major oxide plots of NCIR basalts. Grey square- NCIR data from literature, solid grey circle- VT basalts, Solid black square- VM basalts (data from Table 4).

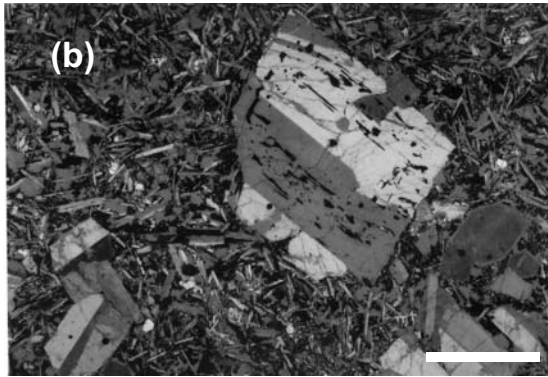
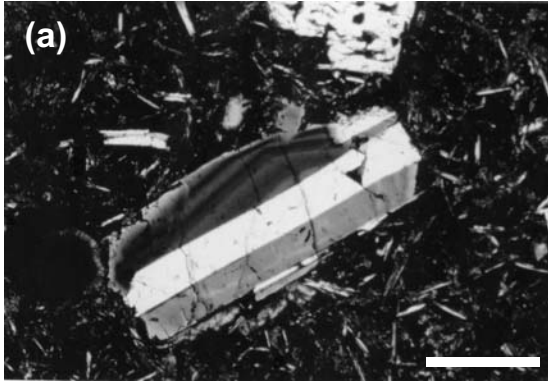
Fig. 6. Plots of some selected trace elements against magnesian number (#Mg), symbols as in Fig. 5.

Fig. 7a-c. CI Carbonaceous chondrite normalised (after McDonough and Sun, 1995) REE plots of NCIR basalts, a,b and c represent the VT 4, VT 5 and VM 9DG samples respectively. Figs 7d-f represent the binary plots of total REE vs #Mg, TiO_2 and P_2O_5 , bars in figure (e) represent variations in TiO_2 contents of Type-I, II, III Indian Ocean

basalts, after Natland (1991). Solid grey squares in Figs. 7d-f represent the present dataset of NCIR basalt.

Fig. 8. Plot of the NCIR primary basalts in the normative Ol-Di-Qz diagram projected from plagioclase apex (after Walker et al., 1979). Solid square- NCIR primary basalt. Solid grey square-fractionated basalt, for data source see Table 4. ol-olivine, au-augite, opx-orthopyroxene.





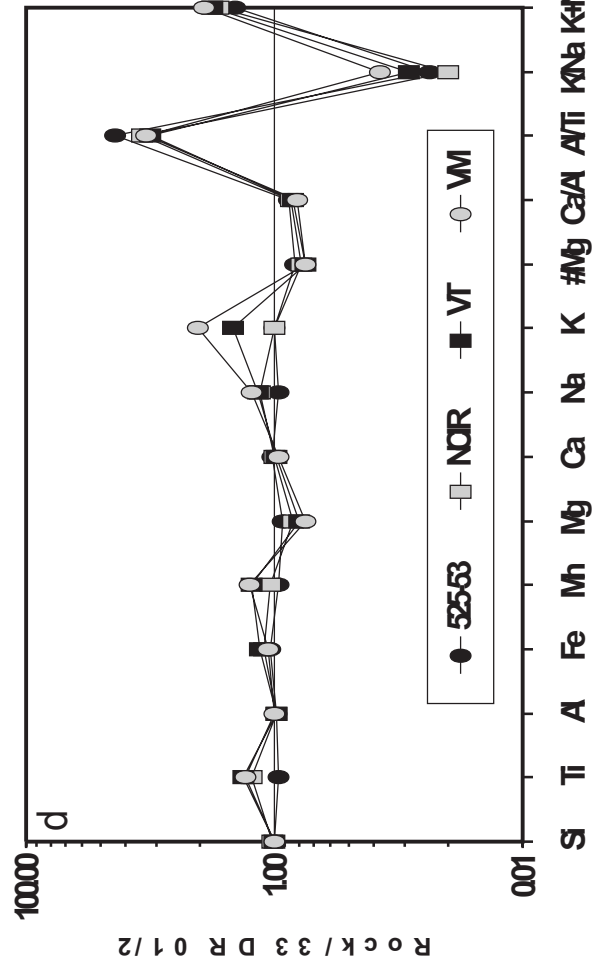
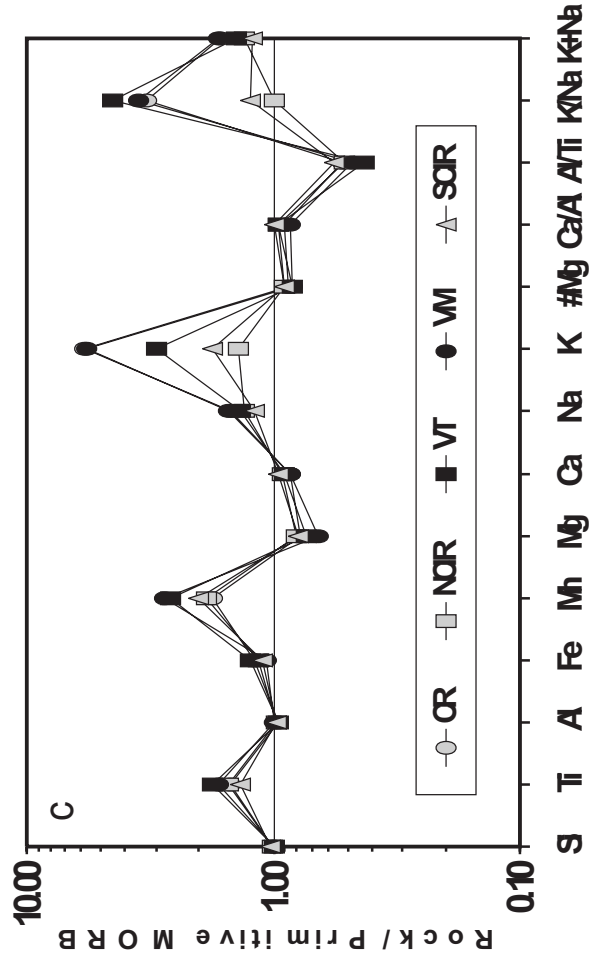
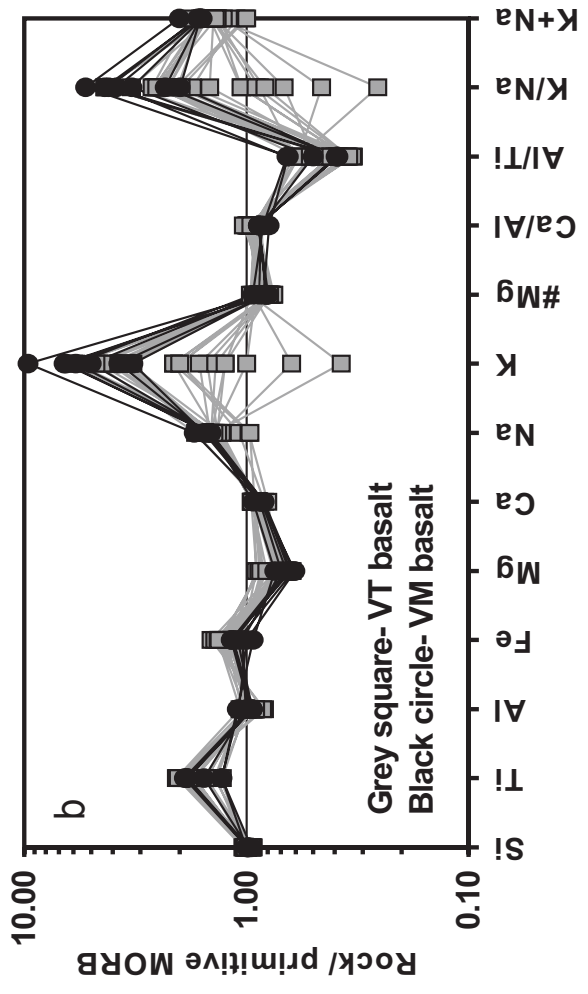
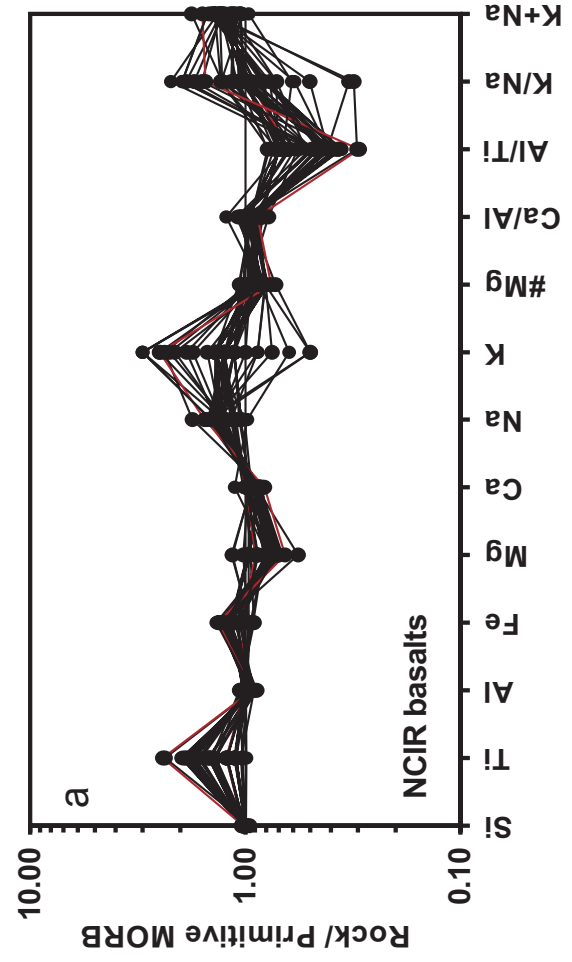


Fig. 3

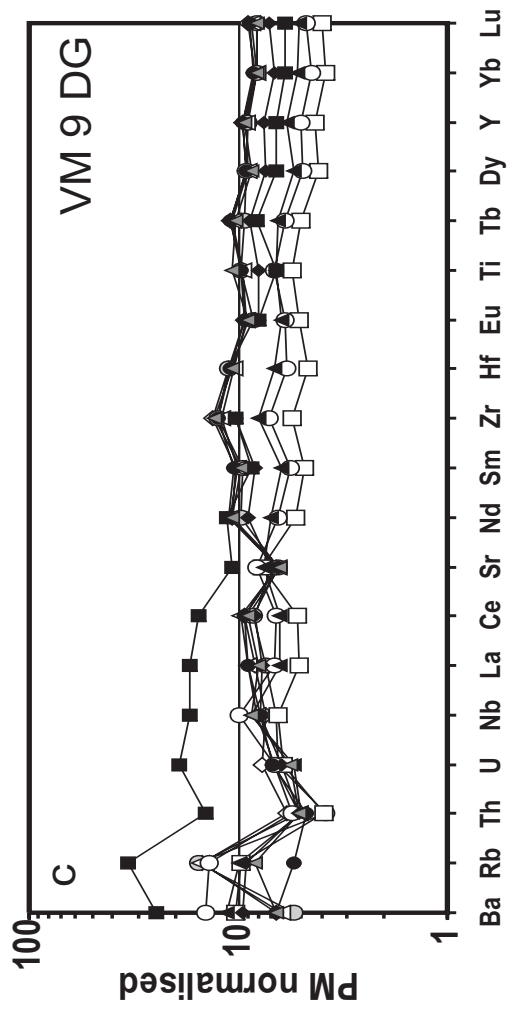
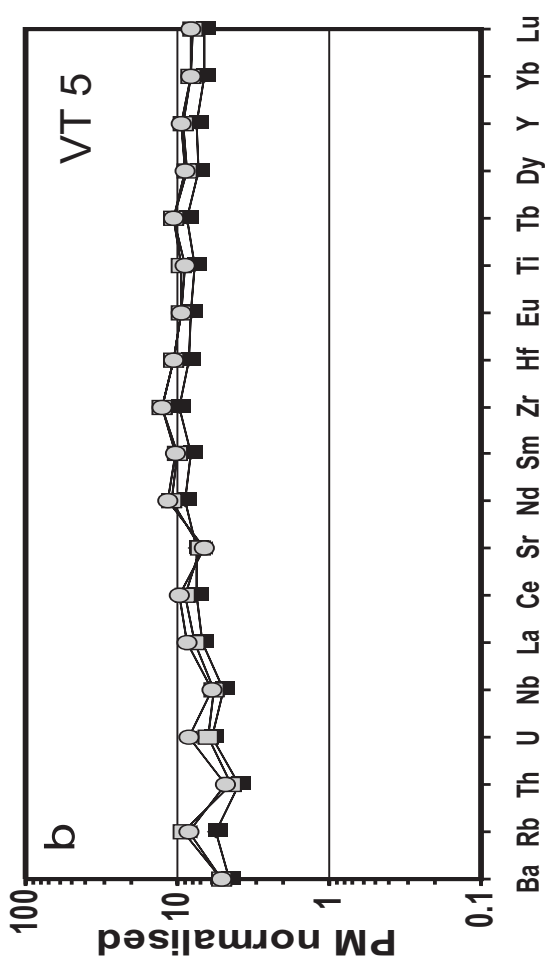
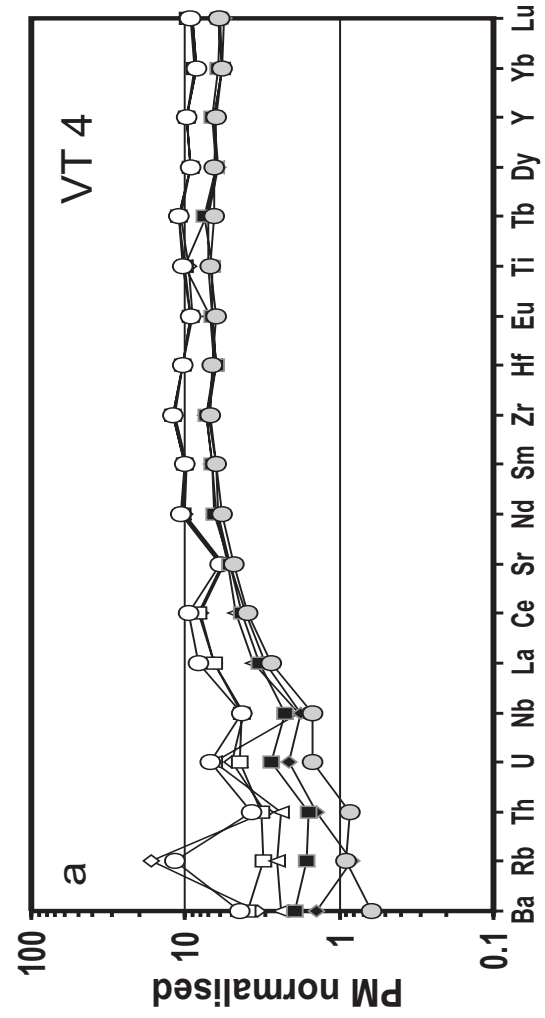


Fig. 4

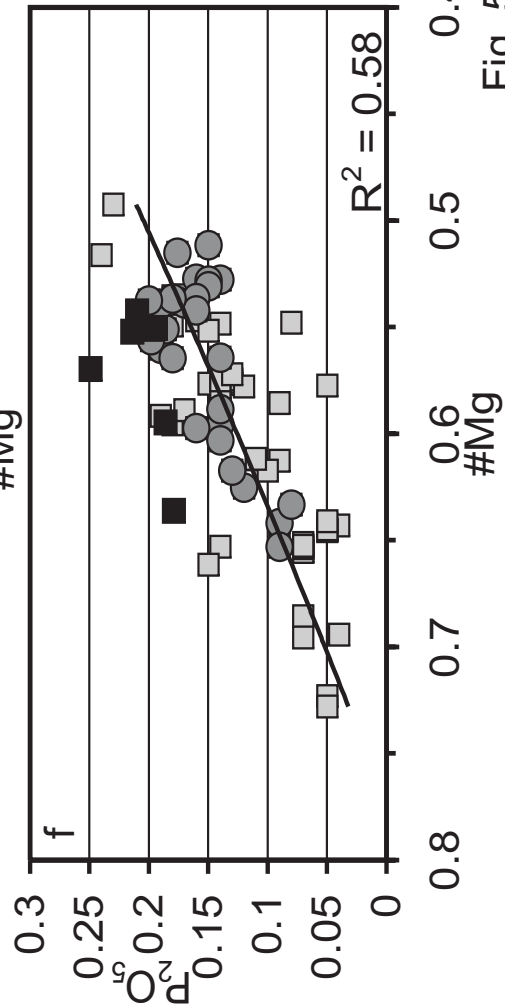
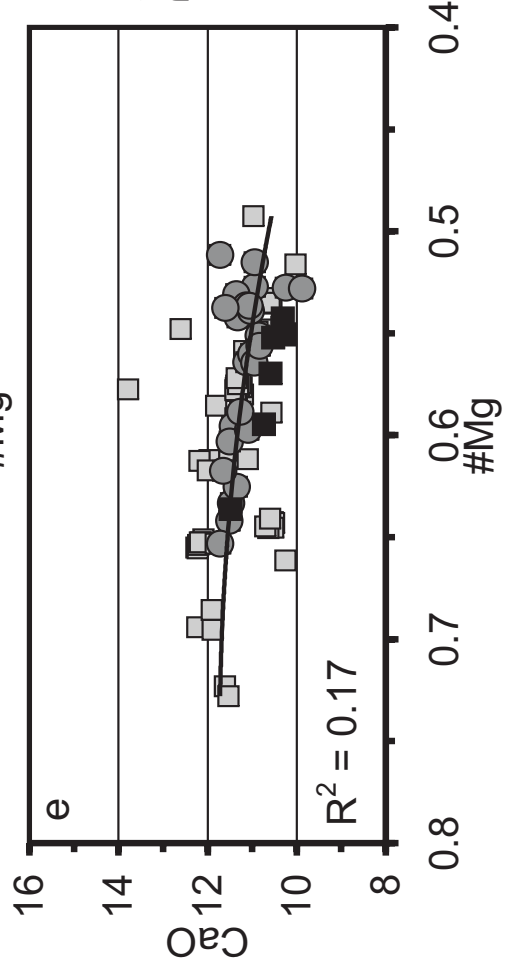
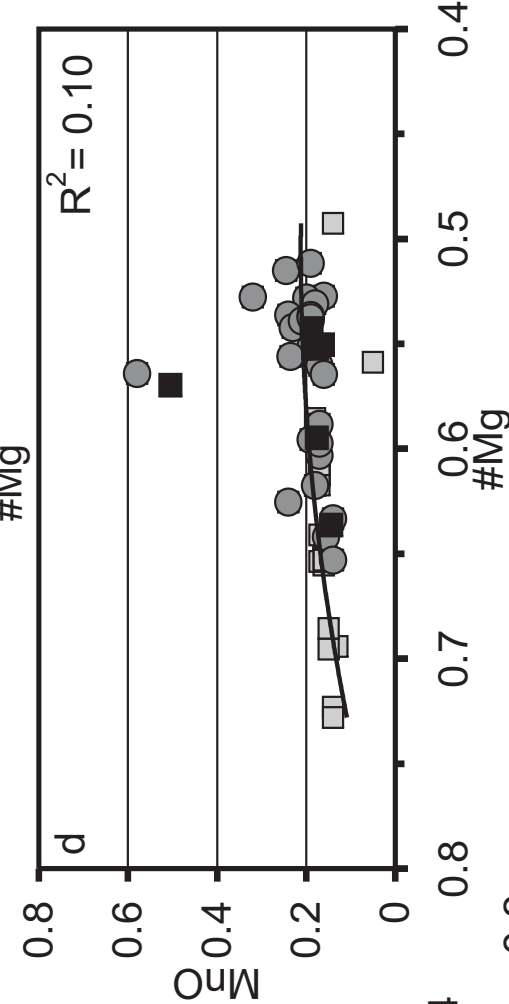
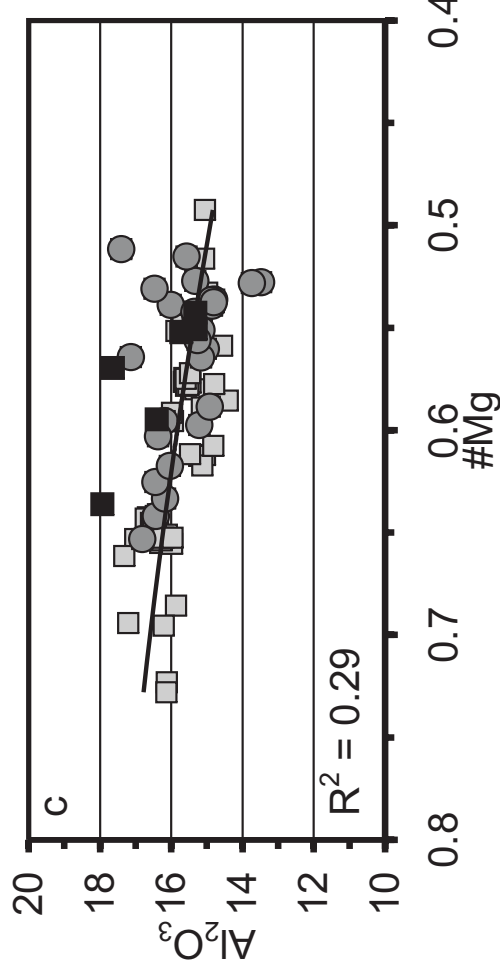
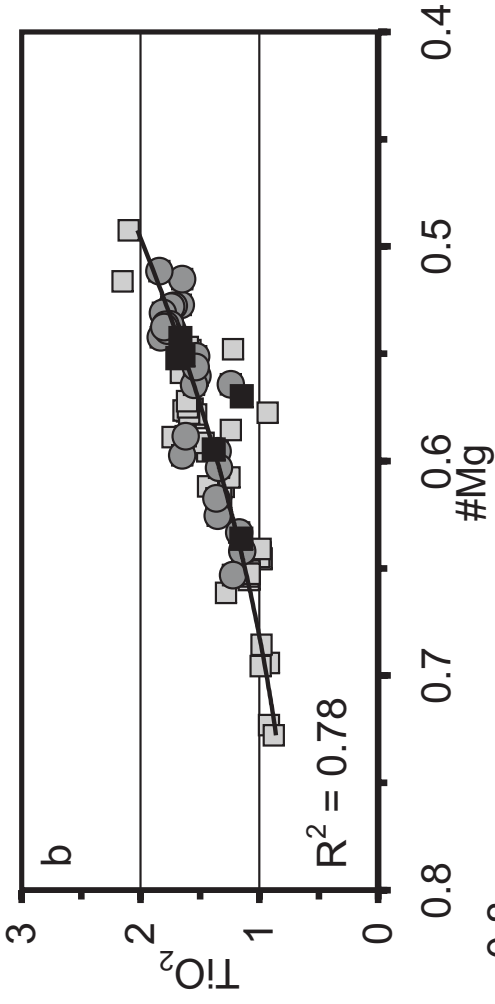
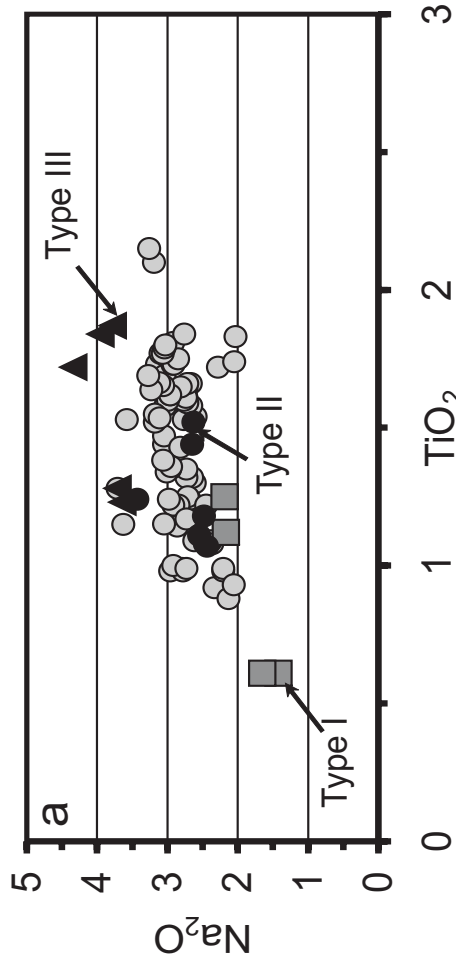


Fig. 5

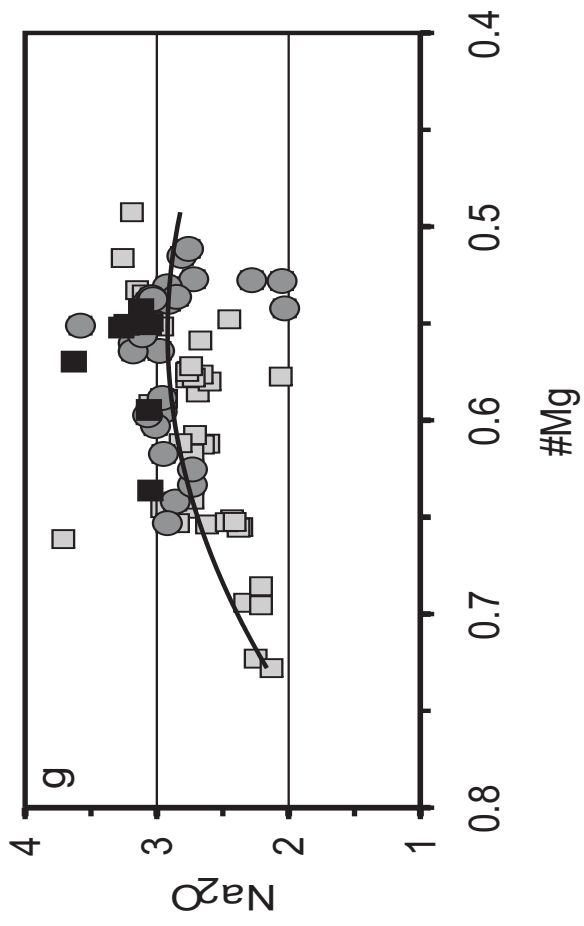
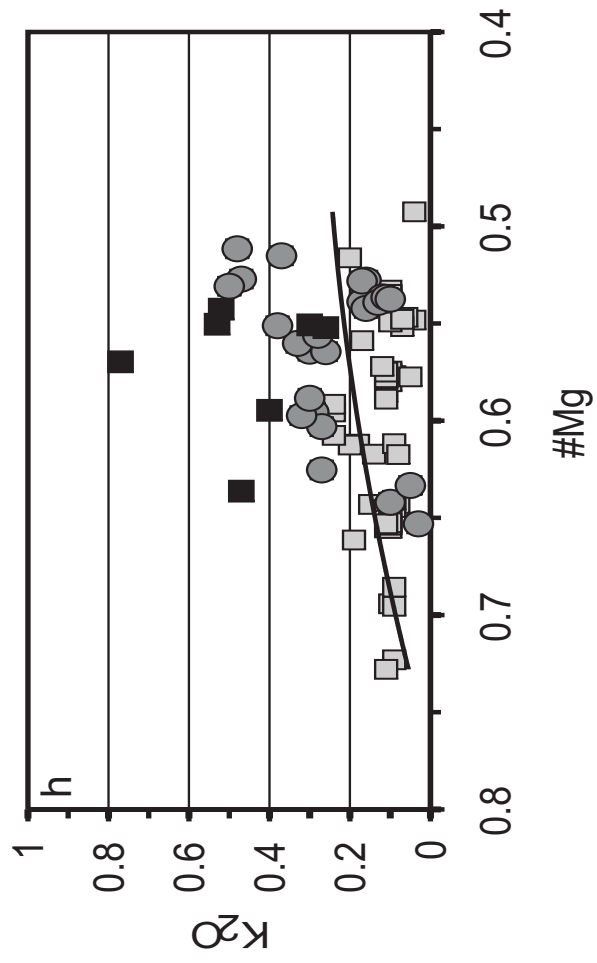


Fig. 5

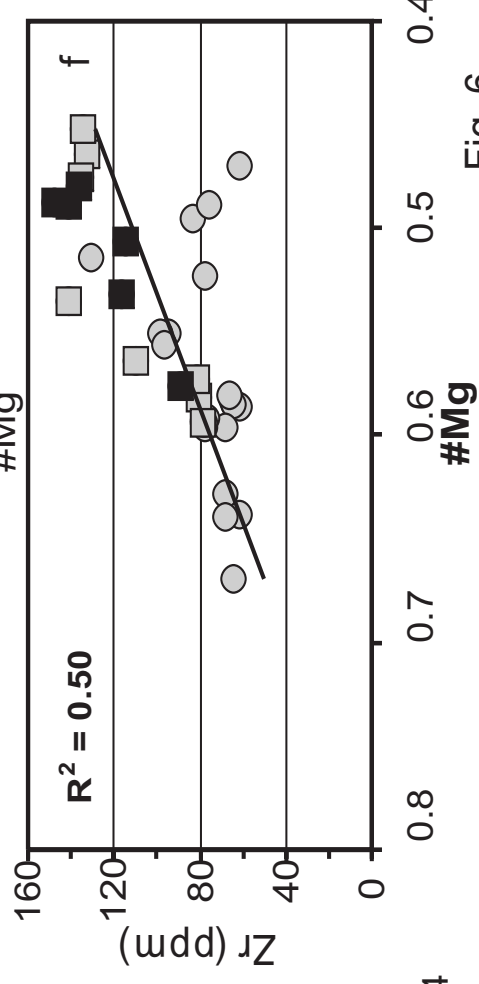
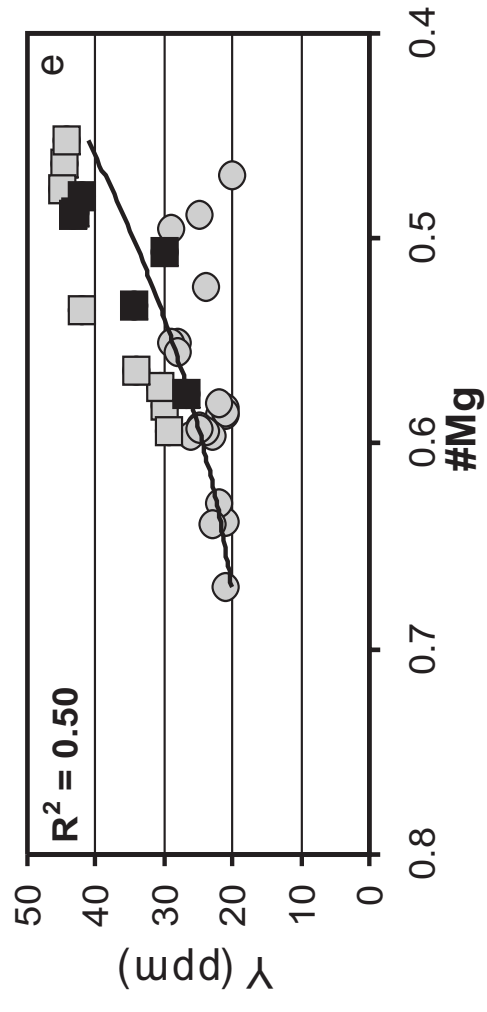
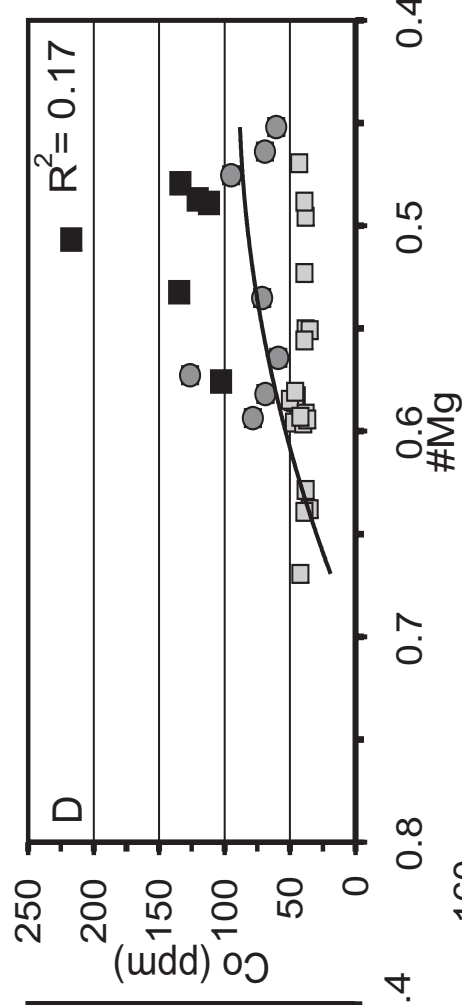
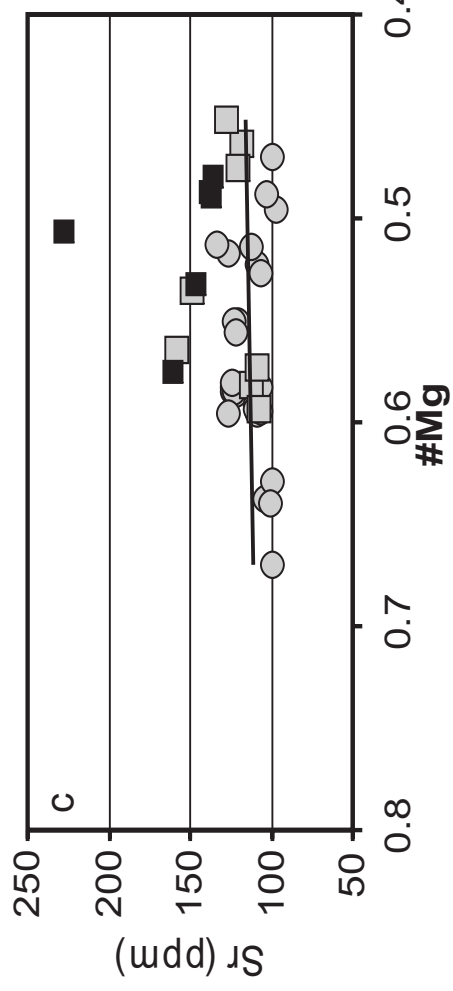
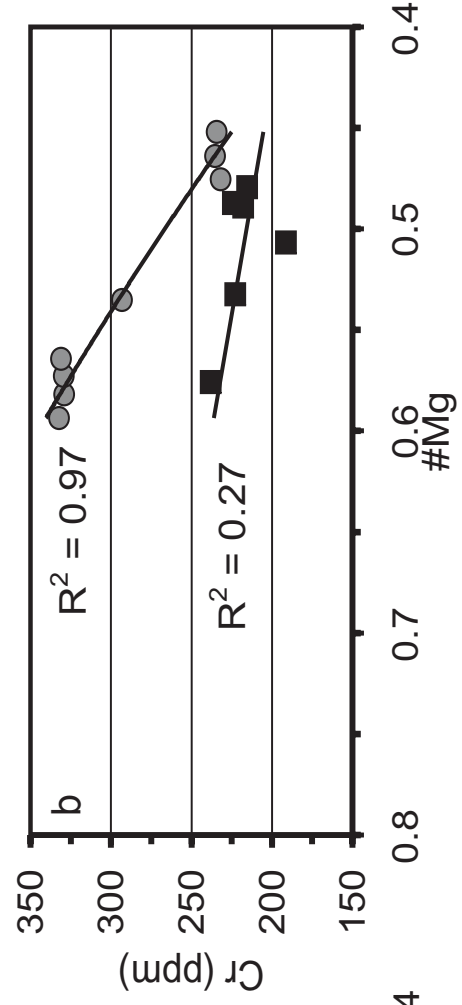
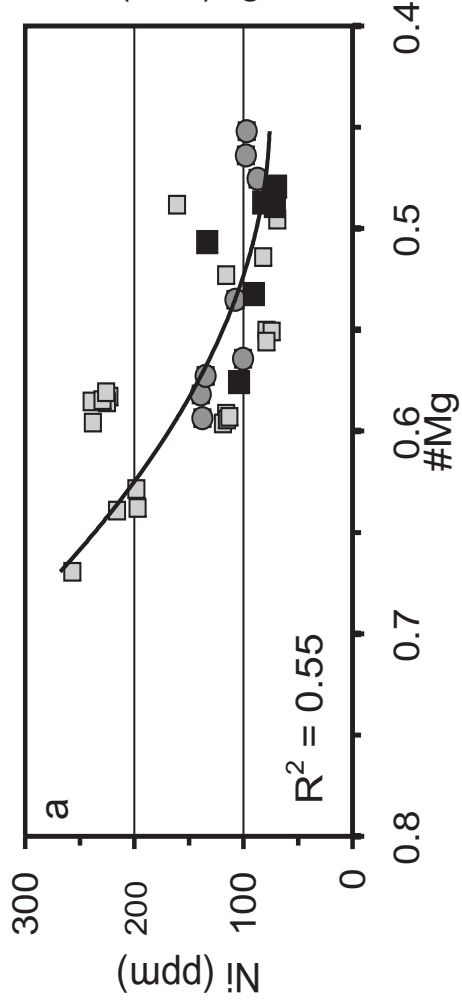


Fig. 6

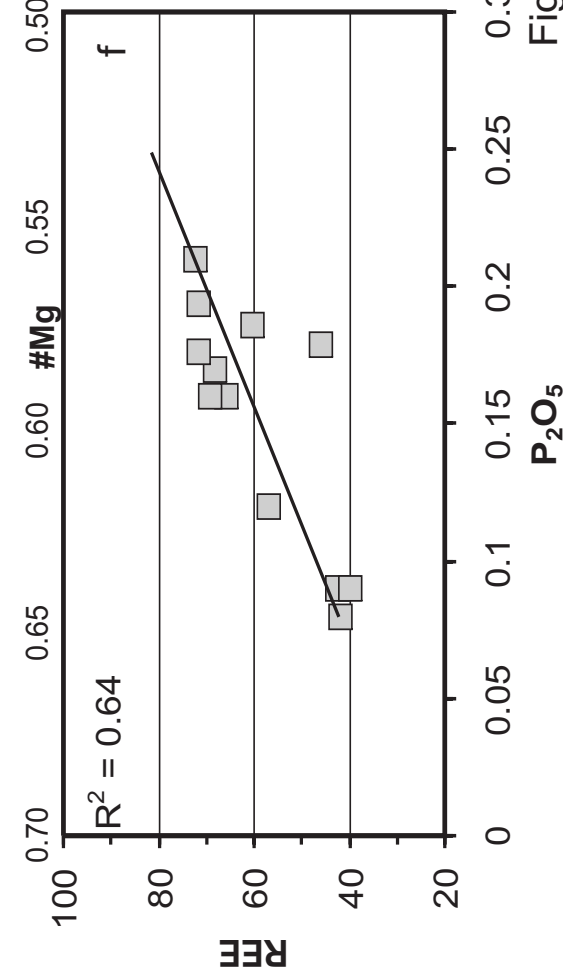
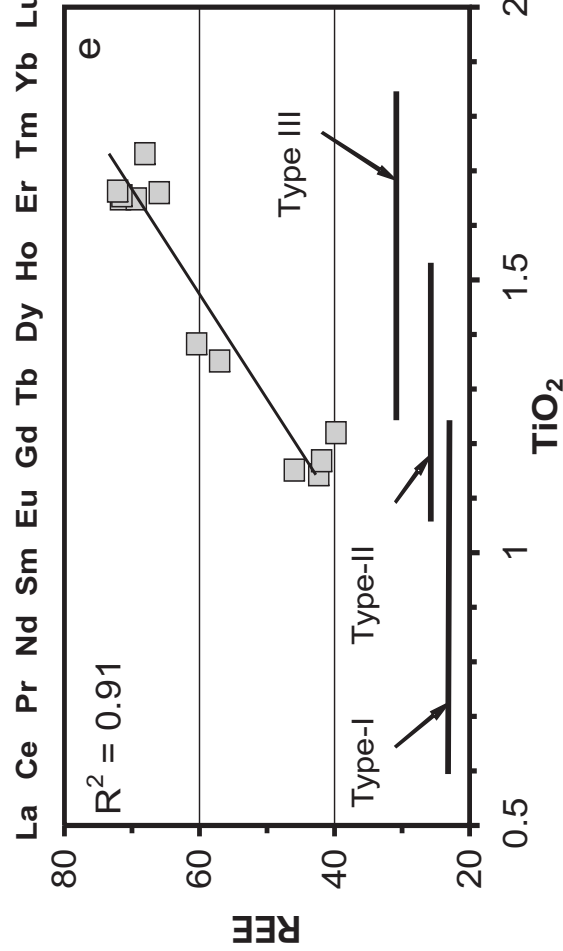
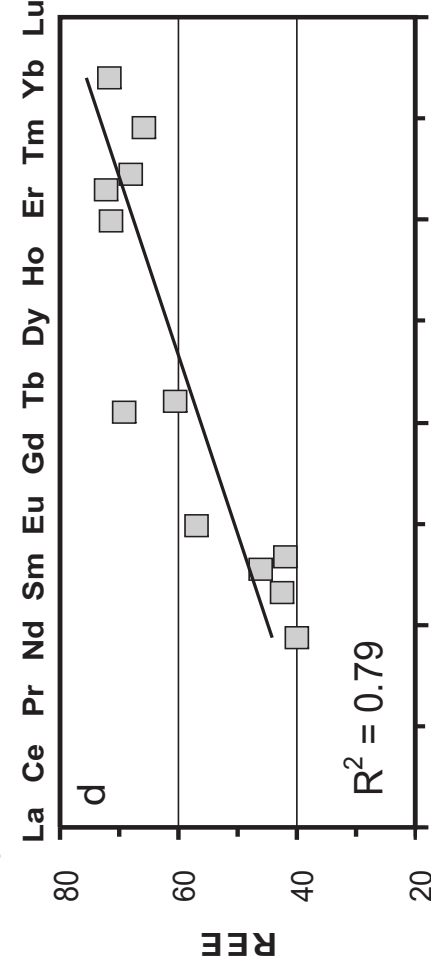
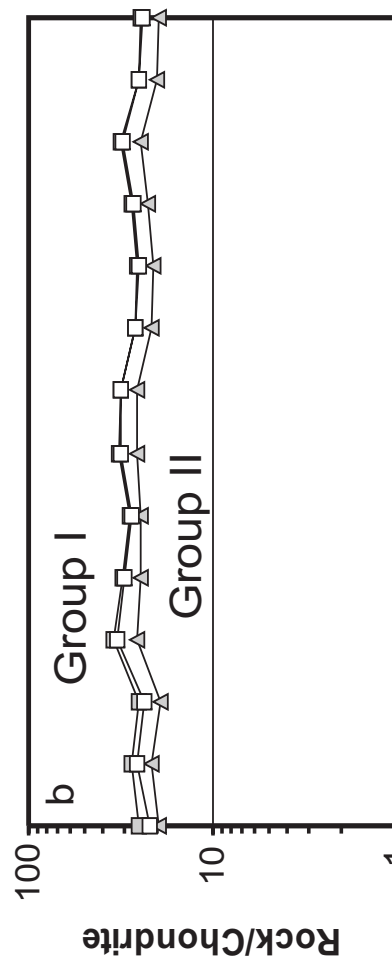
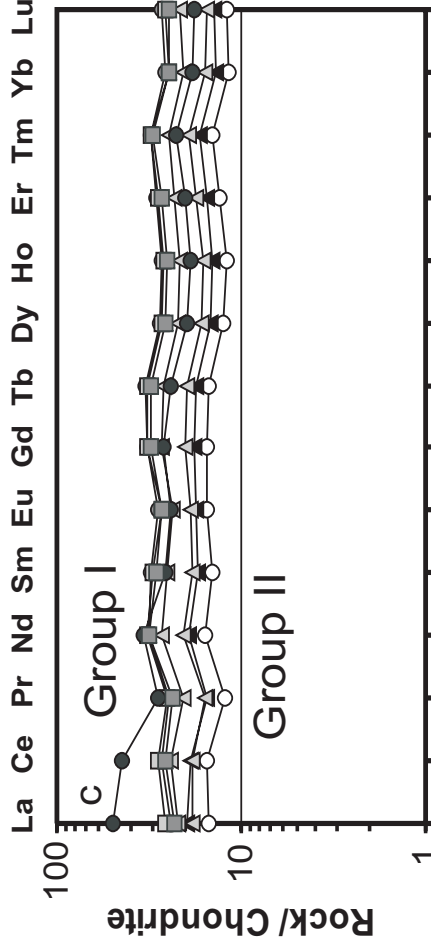
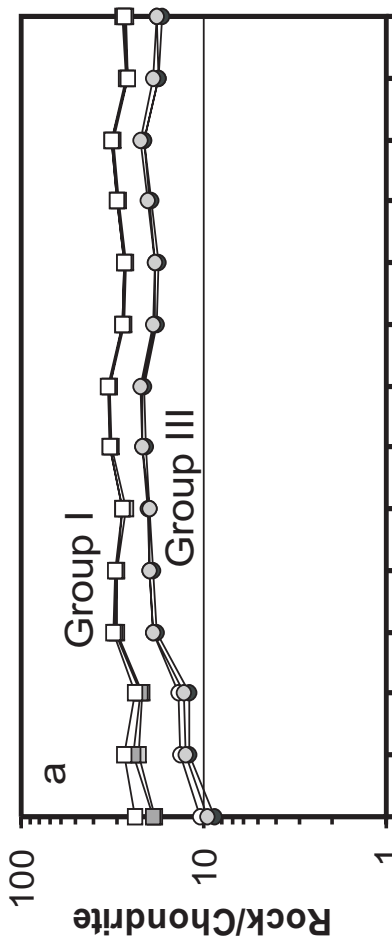


Fig. 7

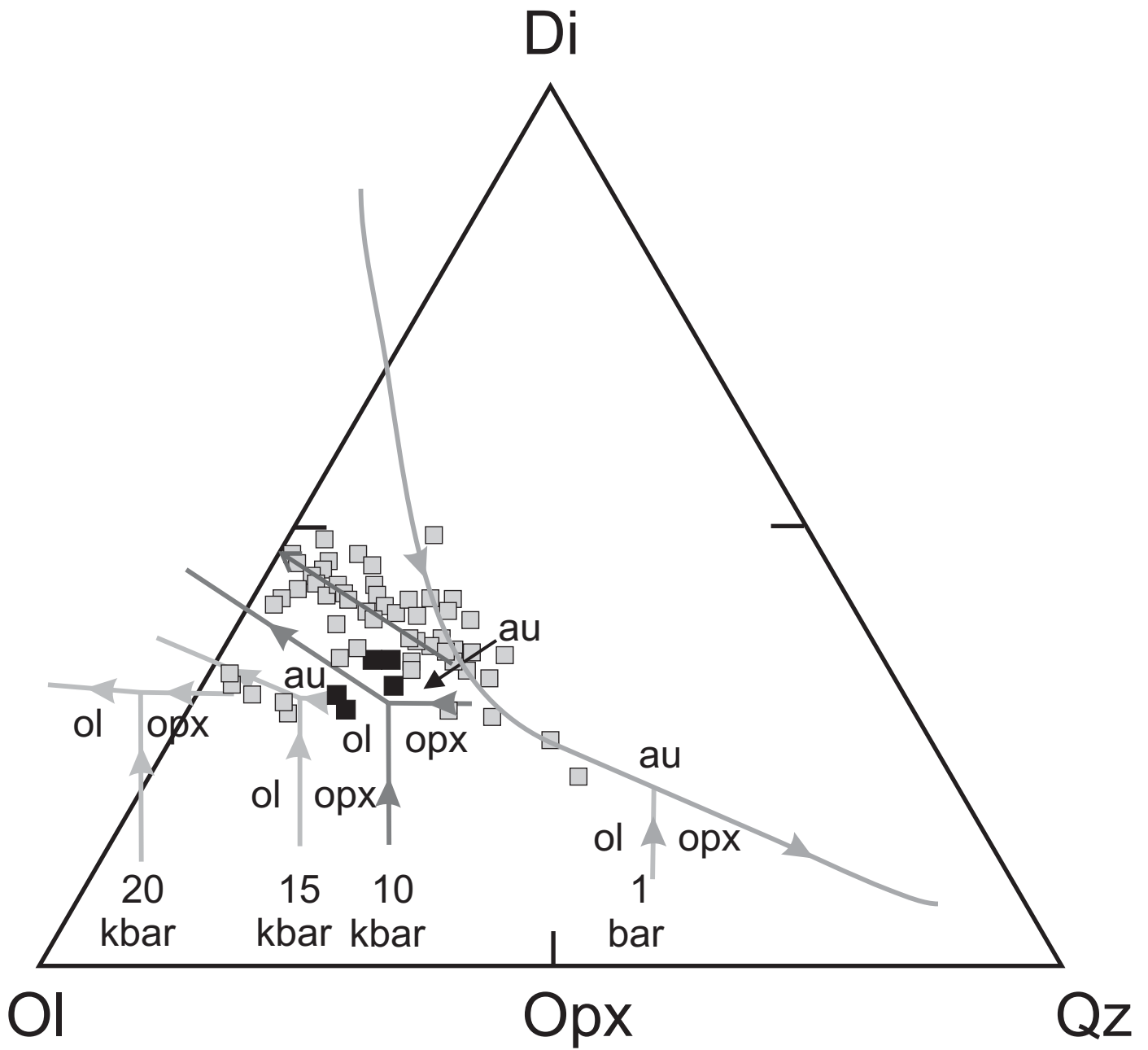


Fig. 8